



## Tansley review

# The shaping of plant axes and crowns through tropisms and elasticity: an example of morphogenetic plasticity beyond the shoot apical meristem

Author for correspondence:  
Bruno Moulia  
Email: [bruno.moulia@inrae.fr](mailto:bruno.moulia@inrae.fr)

Received: 30 September 2020  
Accepted: 17 June 2021

**Bruno Moulia<sup>1</sup>** , **Eric Badel<sup>1</sup>** , **Renaud Bastien<sup>1,2</sup>** , **Laurent Duchemin<sup>3</sup>**   
**and Christophe Eloy<sup>4</sup>** 

<sup>1</sup>Université Clermont Auvergne, INRAE, PIAF, F-63000 Clermont–Ferrand, France; <sup>2</sup>INSERM U1284, Center for Research and Interdisciplinarity (CRI), Université de Paris, F-75004 Paris, France; <sup>3</sup>Physique et Mécanique des Milieux Hétérogènes, CNRS, ESPCI Paris, Université PSL, Sorbonne Université, Université de Paris, F-75005 Paris, France; <sup>4</sup>Aix Marseille Univ, CNRS, Centrale Marseille, IRPHE, F-13013 Marseille, France

## Contents

Summary	2354	V. What controls the shaping of the crown edge?	2371
I. Introduction	2355	VI. Conclusion	2375
II. On growth, shapes and form	2355	Acknowledgements	2377
III. Genetic and environmental control on crown and axis shapes	2357	References	2377
IV. What does control the shaping of each axis?	2359		

*New Phytologist* (2022) **233**: 2354–2379  
doi: 10.1111/nph.17913

**Key words:** biophysics, *LAZY*, modelling, morphogenesis, shoot, *TAC1*, tropism, *WEEP*.

## Summary

Shoot morphogenetic plasticity is crucial to the adaptation of plants to their fluctuating environments. Major insights into shoot morphogenesis have been compiled studying meristems, especially the shoot apical meristem (SAM), through a methodological effort in multiscale systems biology and biophysics. However, morphogenesis at the SAM is robust to environmental changes. Plasticity emerges later on during post-SAM development. The purpose of this review is to show that multiscale systems biology and biophysics is insightful for the shaping of the whole plant as well. More specifically, we review the shaping of axes and crowns through tropisms and elasticity, combining the recent advances in morphogenetic control using physical cues and by genes. We focus mostly on land angiosperms, but with growth habits ranging from small herbs to big trees. We show that generic (universal) morphogenetic processes have been identified, revealing feedforward and feedback effects of global shape on the local morphogenetic process. In parallel, major advances have been made in the analysis of the major genes involved in shaping axes and crowns, revealing conserved genic networks among angiosperms. Then, we show that these two approaches are now starting to converge, revealing exciting perspectives.

## I. Introduction

The study of shapes and forms has had a long history in biology, for example d'Arcy Thompson (1917). It has been focused mostly on: (1) the developmental process generating the shape, namely morphogenesis; and (2) the relationship between shapes and functions and the possible adaptive value of a given shape leading to its selection along evolution, for example Niklas (2013) and Vos *et al.* (2010). These views are not exclusive. First it is now clear that the gene action on shapes only occurs along morphogenesis itself (from Waddington, 1957), and that this can then be selected through evolution, for example Harrison (2017) and Nikolov *et al.* (2019). Second, the adaptive value of the shaping may result from the direct influence of the environment on morphogenesis, named phenotypic plasticity. The situation of shaping is indeed very different in plants and animals. Animal morphogenesis occurs mostly during the embryogenic stage, with some further limited allometric changes during juvenile growth. Plants, in contrast, are characterised by an indefinite growth all throughout their life. In addition, they are usually fixed in a given area and a large part of their adaptation to their current environment goes through growth and shaping. However, the majority of the studies of the morphogenesis in plants has been centred on a few early growth stages. Considering land angiosperm dicots and the morphogenesis of the shoot system, two specific aspects of the development have been mostly studied.

First is the development of the embryo in the seed (e.g. Creff *et al.*, 2015; Fig. 1a). Although displaying a common core and very distinct stages of development at dormancy among species, embryo development usually only sets two meristematic poles (i.e. 'stem cells budding') namely the shoot apical meristem (SAM) and the root apical meristem (RAM). However, there is still a long way to go to explain the shape of a big tree.

Beyond embryogenesis, a particular attention has also been given to the SAM (Fig. 1b–f; Wang *et al.*, 2018; Schnablova *et al.*, 2020). The SAM is involved in bulging of leaf primordia (P) in its superficial layers, and the building of phyllotaxis (Fig. 1b). Extensive systems biology and biophysics allowing an integrative and quantitative understanding of this dynamic system with its different levels of biological organisation has been conducted. It has worked out the interplay of: (1) the chemical signalling by auxin; (2) mechanical signalling; and (3) growth biomechanics, leading to the emergence of successive leaf primordia and their arrangement into a phyllotactic pattern (Smith *et al.*, 2006; Hamant & Traas, 2010; Murray *et al.*, 2012). The key controlling parameters have been defined through a biophysical approach (Douady & Couder, 1996a,b). Then, the key regulating gene networks have been unravelled (Paul *et al.*, 2014; Traas, 2018; Wang *et al.*, 2018). It was found that this phyllotactic pattern is particularly stable (Truskina & Vernoux, 2018), protected and buffered from external influences. This occurs by involving shape-feedback and mechanosensing mechanisms that reduce the amount of possible shapes (Smith, 1978; Hamant & Mouliia, 2016). Altogether, SAM research has involved a tight coupling of modelling, imaging and focused experiments in a remarkable exercise of multiscale systems

biology and biophysics. Similar methods are now starting to be applied to the rib zone just below the SAM (Serrano-Mislata & Sablowski, 2018; McKim, 2020; Fig. 1c) where homeobox genes drive the segmentation into phytomers (Fig. 1d,e), with the node matching the developing leaf primordium and the axillary meristem ( $A_xM$ ; Serrano-Mislata & Sablowski, 2018; Wang *et al.*, 2018; Fig. 1c,d).

The purpose of this review is to show that a multiscale systems biology and biophysics approach can also be used to study the post-SAM aerial morphogenesis of plants, including trees. Through the use of models integrating the major physical factors and signals involved, this approach allows the unravelling of how the dynamics of shoot morphogenesis can give rise to genetically stable patterns, while displaying a considerable plasticity. The feedback from the global shape (of the axis, the crown, etc.) to local shaping mechanisms can be analysed. Then, the key parameters controlling that morphogenesis can be defined and traced back to controlling cells and gene networks. Finally, the way these parameters, and their genetic control through allelic variation, may have been selected along their evolution can be envisioned.

However, post-SAM morphogenesis is a very large subject. Recent reviews are available describing the processes at the level of: (1) the rib meristems (van der Schoot *et al.*, 2014; Serrano-Mislata & Sablowski, 2018; McKim, 2020); (2) the development of phytomers (Fig. 1d; McSteen & Leyser, 2005; Vos *et al.*, 2010); (3) the control over the branching pattern (Barbier *et al.*, 2019); (4) the cambium (the meristem responsible for the secondary diameter growth and wood production in dicots; Fig. 1c) and its involvement in morphogenesis (Spicer & Groover, 2010; Hartmann *et al.*, 2017; Ragni & Greb, 2018); and (5) the global architecture (Barthelemy & Caraglio, 2007) and its control by genes (Costes & Gion, 2015; Wang *et al.*, 2018) and by external cues (Mouliia *et al.*, 2015; Ballare & Pierik, 2017; Eloy *et al.*, 2017).

We will therefore concentrate here on the shaping of the axes and of the crown through tropisms and elasticity, focusing on the recent advances in its control using physical cues and using genes. In the following sections, we will therefore first clarify how to define the shape(s) of plant axes and crowns. Then, we will review some of the major genetic and environmental controls of crown and axis shapes and identify the missing links that a multiscale approach involving systems biology and biophysics has to address. We will then study what controls the shaping and orientation of each single axis and the resulting shaping of the crown edge, at various developmental stages.

In every aspect, we put the emphasis on: (1) the understanding of the core of the dynamics involved; and (2) the identification of generic (universal) morphogenetic processes involving both physics and biology, through modelling. We will also try to start making a link with some of the major genes known to affect the shaping of the shoot system.

## II. On growth, shapes and form

Morphology means 'discourse about' form and shape, whereas morphogenesis means the generative process shaping the plant.

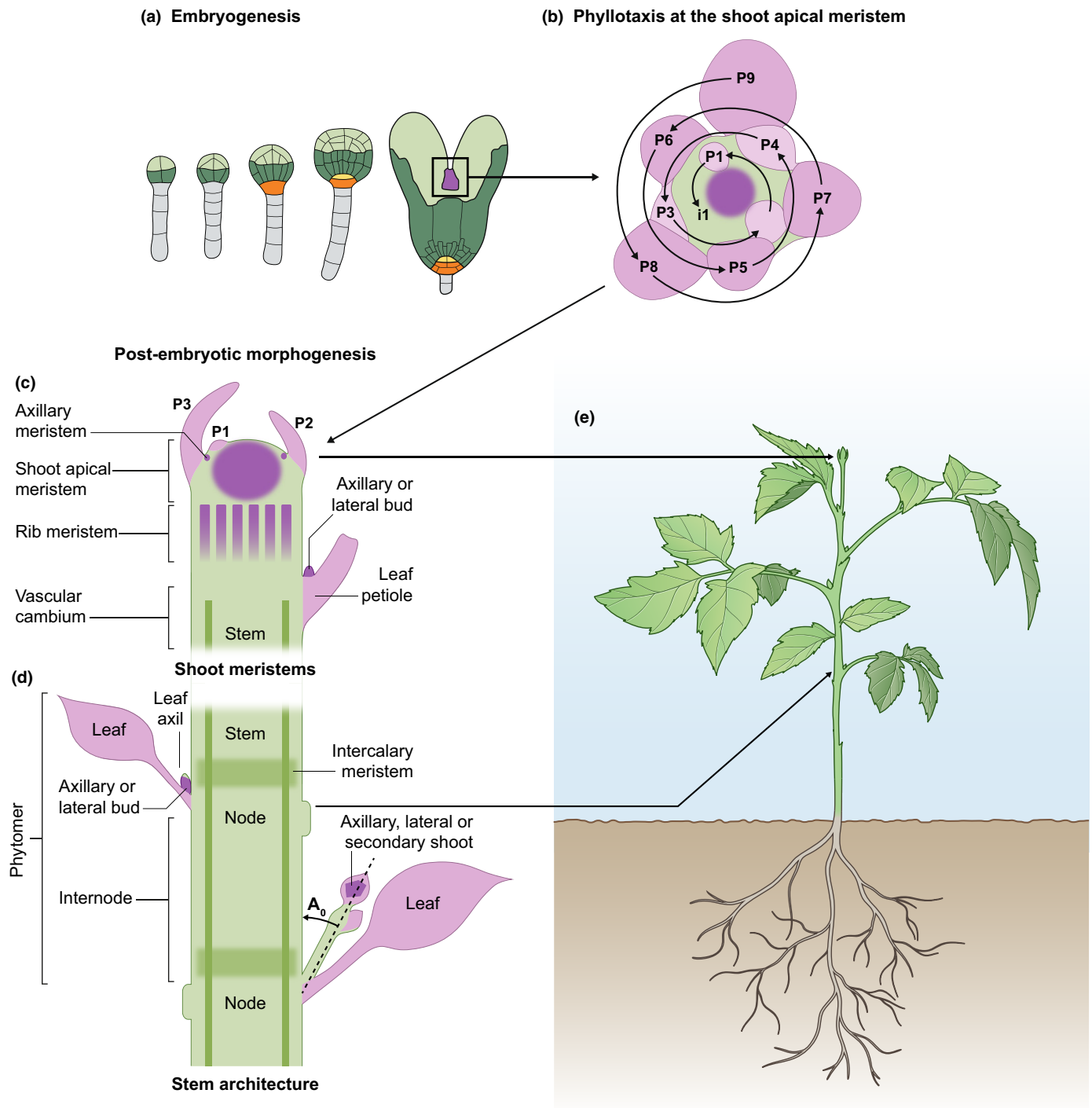


**Fig. 1** The major stages of early plant development in land angiosperms. (a) Early embryo development in *Arabidopsis thaliana* (with the central zone of the shoot apical meristem (SAM) in purple). (b) Top view of the SAM in *Arabidopsis thaliana* with the phyllotactic patterning of the leaf primordia ( $P_i, i = 1-9$ ). (c) Schematic view of a longitudinal cross-cut of the SAM showing the SAM and leaf primordia, but also the differentiation of the axillary meristems (AMs) at the boundary zone of the leaf primordia and the functioning of the subapical rib meristem producing cell extension and phytomer differentiation, with the segmentation of the stem into phytomers; and finally the secondary dedifferentiation of a circumferential meristem dedicated to long-term radial growth of the stem: the cambium. (d) Schematic view of a stem organised into a modular set of segments called phytomers (i.e. an internode, a node, the subtending leaf and its axillary bud). (e) A typical young dicot with the location of its SAM and phytomers, as well as the onset of branching when an AM becomes active as a new SAM, producing a lateral axis with a insertion angle  $A_0$ . (a) From Radoeva & Weijers (2014). (b) Modified from Murray *et al.* (2012). (c-e) Modified from Wang *et al.* (2018).

Shape and form can be synonymous; but in the following sections we will consider that the shape describes the outer contour of a form described by its topology and geometry (Godin, 2000). For

example, for a tree crown, its envelope can define its shape, whereas its form can be defined only when also considering the subtending internal branched architecture.

It is also important to realise that shape and size are different things. Two objects can have the same shape but different sizes (Fig. 2a).

Shape can only be characterised by dimensionless quantities (Niklas & Cobb, 2017), in which the effect of size is cancelled out. For example the slenderness or aspect ratio of the length/basal radius  $L/R_0$  is dimensionless (Fig. 2a). When considering a growing plant axis, one may also consider the length of the growth zone  $L_{gz}$  (the zone in which cell expansion growth occurs in the wake of the rib meristem; Fig. 1c) and the radius at the basis of the growth zone  $R(s = (L - L_{gz}))$ , so the dimensionless aspect ratio of the growth zone becomes  $L_{gz}/R(s = (L - L_{gz}))$  (Fig. 2b,c). Angle  $A$  (Fig. 2b) is also dimensionless (measured in radians, the ratio of the arc length to the radius). Curvature  $C$ , the rate of change of angle with spatial position  $s$  along a line ( $C = \partial A/\partial s$ ; Fig. 2d) is not dimensionless (its unit is  $m^{-1}$ ); but the product  $C \times R$ , where  $R$  is a typical radius for the system being considered (Fig. 2c), is a dimensionless shape characteristic. Then the shape of a plant axis at a given time  $t$  can be defined as the spatial distribution of its curvature  $C(s)$  (Fig. 2d), or more precisely, its dimensionless version  $\tilde{C}(s, t) = C(s, t)R$  (where  $R$  is a typical radius of the axis; Fig. 2a,c).

Shapes are also often characterised by the exponent of the scaling relation between two geometric characteristics of the object, as for example the scaling relations between: (1) the length  $L$  and the basal radius  $R_0$   $L = k_1(R_0)^{\theta_1}$  of an axis (Fig. 2a) or the total height  $H$  of a tree and the radius (or diameter) at breast (chest) height of its trunk  $H = k_2(R_0)^{\theta_2}$  (Fig. 2f), both defining the slenderness of these objects or (2) the diameter of the trunk and the size of the crown (often approximated through crown diameter  $D_c$  or the total leaf mass  $M_{\text{foliage}}$ )  $D_0 = 2R_0 = k_3(M_{\text{foliage}})^{\theta_3}$  (Fig. 2e,f). Establishing these scaling relationships requires measuring the two traits over many plant axes (for example of many branches or trunks, from  $L$ ,  $R_0$  (Fig. 2a) or  $h$ ,  $R_0$  (Fig. 2f)). Another length–width relationship can be established by measuring the width over many places along the object (from the radius of an axis  $R$  as a function of the spatial position  $s$  along it), defining its tapering  $R(s)$ , as for example  $R(s) = R(L) + (R(0) - R(L))(1 - \frac{s}{L})^\zeta$  (Fig. 2a).

When these relationships take the form of a power law, such as  $(R) = a \cdot R^{-\delta}$ , they are invariant by scaling by a factor  $k$  (i.e.  $(kR) = a|k|^{-\delta} \cdot L(R)$ ). In biology, such a relationship is called an allometry. This has received intensive coverage and allometries for axis and crown shapes (slenderness, tapering, etc.) have been defined on empirical and theoretical grounds (see Niklas, 1994; Mouliia & Fournier, 1997; Niklas & Spatz, 2004; Eloy *et al.*, 2017 for critical reviews).

Crown shape has long been described only qualitatively through the mere distinction between ‘excurrent’ crowns (i.e. ‘cone’ shaped, with a central leader; Fig. 2e) vs ‘decurent’ crowns (rounded or spreading, with multiple scaffold branches; Fig. 2f). Arboriculturists have refined this typology into four classes (conical, domed, ellipsoidal, oval), further refined according to the crown slenderness (e.g. broad dome vs narrow dome, rounded vs columnar ellipsoid) and/or its tapering (aboval vs oboval) (Fig. 2g; Lenard, 2008). Light-exchange modellers have proposed a series of 3D shapes describing quantitatively crown shapes in trees (Fig. 2h,i). It was

found that outlines can often be described with fairly regular convex geometrical shapes when considering isolated trees or shrubs (Marin-Buzon *et al.*, 2020; Fig. 2h); whereas irregular polyhedrons are necessary for crowns inside canopies (Krucek *et al.*, 2019; Fig. 2i) or in conditions with directional light or winds.

While size and shape are different things, they can be biologically dependent. They are functions that depend on both size and shape (Vos *et al.*, 2010). A selective pressure on these functions along evolution will therefore act simultaneously on size and shape as revealed in the allometric scaling laws (Niklas, 1994; Mouliia & Fournier, 1997; Eloy *et al.*, 2017; Lehnebach *et al.*, 2018).

### III. Genetic and environmental control on crown and axis shapes

Crown shape and the pattern of axes are usually considered as genetically heritable habits (Barthelemy & Caraglio, 2007; Lenard, 2008). This genetic effect on crown shape of isolated trees is so strong that the landscape architects Cesare Leonardi and Franca Stagi in their famous book *l'Architettura degli Alberi* (tree architecture) (Leonardi & Stagi, 2019) have compiled the crown shape habit of 212 species of trees for their use in landscape design. Among these, two classes of crowns in terms of architectural development should be distinguished. In some architectural models, the crown is separated into multiple storeys. In others, the crown seems compact and its outline can be defined objectively as a smooth surface. In the following, we will concentrate on the second type that corresponds to very numerous species.

Major insight has been obtained into some of the major genes controlling the shaping of axes and crowns. Three highly conserved homologous genes (or gene family) *TAC1*, *LAZY* and *WEEP* have become major players in shoots in many species (Hollender & Dardick, 2015; Hill & Hollender, 2019; Hollender *et al.*, 2020). Here, we focus only on their ‘phenotypic effect’ on branch shaping and on the missing links between the phenotype and the genotype. When *TAC1* is actively expressed, the lateral branch angle is larger (more plagiotropic branches, see Fig. 3(a–c) for examples in *Arabidopsis*, poplar and plum tree), with no effect on the main axis. The crown is broader. When *TAC1* is inhibited (*tac1*), the lateral shoots are closer to the vertical, leading to a columnar (‘fastigiated’) crown habit (Fig. 3d–f). By contrast, when genes from the *LAZY* family are actively expressed, the angle of the lateral branches becomes steeper. Finally, when the *WEEP* gene is highly expressed, the lateral branches, as well as the main stem, are straight, whereas all of these axes bend downwards actively in the *weep* mutant. Note that this effect of the *weep* mutation has been demonstrated in peach and plum trees (both belonging to the *Prunus* genus), but was not found to be efficient in *Arabidopsis* (Hollender *et al.*, 2018a). Even in tree species, the full genetic and molecular analysis of the weeping phenotype in many species (e.g. poplar; Fig. 3g) is still in progress (Hollender *et al.*, 2018a; Mao *et al.*, 2020; van Es, 2020).

Hypothetical models for the mechanisms of the regulation of branch orientation and crown shaping by these genes involve *TAC1* and *LAZY* as antagonistic actors into sensing of branch orientation vs gravity (gravitropism), modulating the transport of the growth hormone auxin. However the nature of this interaction remains

unclear (Hollender *et al.*, 2020) and *TAC1* shows a limited gravitropic effect (Hollender *et al.*, 2020) and is also related to light (Waite & Dardick, 2018). *WEEP* probably involves another hormonal pathway, gibberellin (van Es, 2020), and it has been shown that the *weep* mutant lacks active gravitropic reorientation

(Hollender *et al.*, 2018a). However, how to relate their molecular and cellular actions to their interactive drive of the shaping of plants axes and crowns by tropisms remains elusive.

In addition, the tree crowns show incredible phenotypic plasticity, varying from one tree to the next, even in clonal plants,

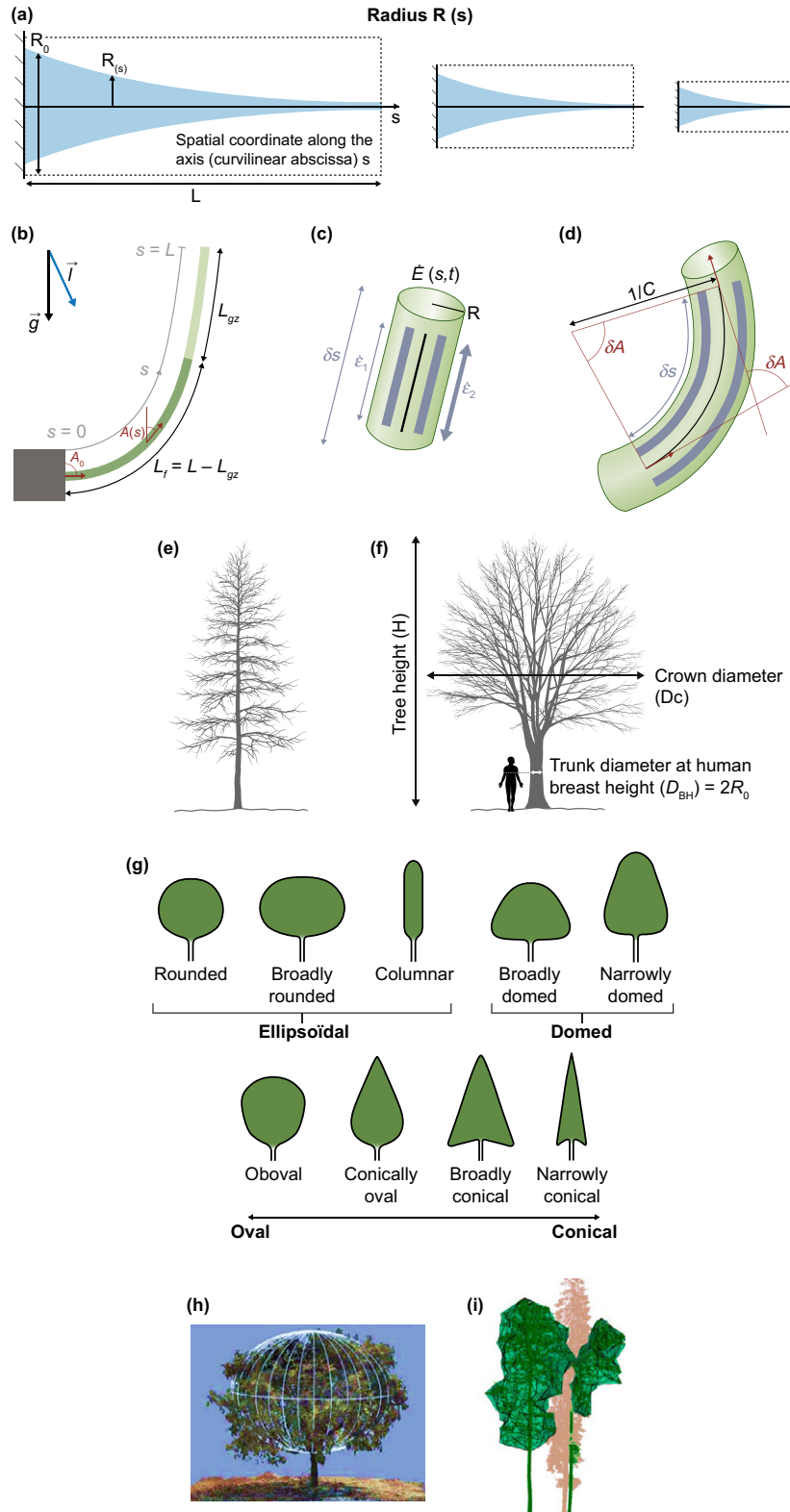


**Fig. 2** Shoot morphometrics. (a) Slenderness (aspect ratio) and tapering: a set of cylinders (dashed lines) and of tapered rods with the same slenderness  $L/R_0$  (isometric scaling) and a 3/2 power-law tapering  $R(s) = R(L) + (R(0) - R(L))(1 - \frac{s}{L})^{3/2}$ . (b) Definitions of the different lengths and angles involved in the analysis of axis tropism: total length  $L$ ; length of the growth zone,  $L_{gz}$ ; length of the 'fixed' mature tissues  $L_f$ ; angle  $A(s)$  between axis and the vertical at curvilinear coordinate  $s$ ; basal angle  $A_0 = A(s = 0)$ ;  $g$ ; gravity acceleration; and  $l$ /light direction. (c, d) Close up of a small axis segment of length  $\delta_s$  and radius  $R$  undergoing curving and elongation growth. (c) The segment is initially straight ( $C = 0$ ) and is undergoing differential growth with growth-induced strain rates  $\dot{\epsilon}_1(s, t) < \dot{\epsilon}_2(s, t)$ . The mean growth rate is  $\dot{E}(s, t) = (\dot{\epsilon}_1(s, t) + \dot{\epsilon}_2(s, t))/2$ . (d) The segment displays nonzero curvature.  $C(s, t)$ , defined as the rate of spatial variation in angle  $A(s, t)$ :  $C(s, t) = \frac{\partial A(s, t)}{\partial s} \sim \frac{\partial A(s, t)}{\partial s}$ . (e, f) Basic botanical typology for crown shapes: excurrent (e) and decurrent (f). In (f) the measurements mostly used for crown shape allometries are shown: total height  $H$ ; trunk diameter at human breast (chest) height  $D_{BH}$ ; corresponding 'basal' radius  $R_0$ ; and crown diameter  $D_c$ . (g) Detailed geometrical typology of crown shapes in isolated trees, based on shape and aspect ratio. (h) Quantitative description of crown shape using 3D envelopes, in sparse tree canopies (orange tree orchard). (i) Quantitative description of crown shape using 3D envelopes, in dense tree canopies with asymmetric and irregular shapes. (a) Redrawn from McMahon & Kronauer (1976); (g) redrawn from Lenard (2008); (h) from Marin-Buzon *et al.* (2020); and (i) from Krucek *et al.* (2019).

according to the environment of each tree, as well as whether it has grown isolated or in group or canopy (Fig. 3h–j). In addition to gravity and gravitropism, the major factors are light and wind. The shape of a crown reflects the position of a given tree within the canopy and the issue of neighbour interactions and competition for space and light (Fig. 3h,i; Krucek *et al.*, 2019). It is now known that this involves sensing of the dimensionless red : far red (R : FR) light ratio in the lateral and zenithal light through phytochrome B (PhyB), as well as on sensing of the amount of blue light (BL); and of course on the effect of the amount of photosynthetically active radiation (PAR) on photosynthesis (Ballare & Pierik, 2017). Lateral light can deform the crown and reorient the axes under phototropism (Coutand *et al.*, 2019). Similarly, indices of crown shape deformation of isolated trees (anemomorphosis) has been taken as an index of (extreme) wind exposure (Fig. 3j; Meneses & Lopes, 2017).

How environment and genetics may interplay in driving the shape of axes and crowns, and how can we approach this issue through a biophysical approach is the ultimate goal of this review. From the biological description above we know that gravitropism and phototropism are key mechanisms, and that their interaction with the light quality and quantity may be also relevant (as long as wind effects are negligible). Let us now start with the shaping of a single axis.

#### IV. What does control the shaping of each axis?

##### 1. The shape of an axis

The most obvious aspect of axis shape is its spatial display. It can be described through its angle of insertion  $A(0)$  and the spatial distribution of its dimensionless curvature  $\tilde{C}(s) = R(s)C(s)$  (Fig. 2b,d). Curvatures can be added step by step along the axis to find all the successive angles  $A(s)$  from the insertion up to the tip angle  $A(s = L)$ . This can be formulated as:

$$A(s) = A(0) + \int_{\sigma=0}^{\sigma=s} C(\sigma) d\sigma \quad \text{Eqn 1}$$

where  $\sigma$  is the dummy integration variable describing the spatial position from the basis of the axis to the actual place of spatial coordinate  $s$  at which the angle  $A(s)$  is calculated. Of course, if  $C(s) = 0$  then the axis is straight and its angle is constant, that is  $A(s) = A(0)$  from  $s = 0$  to  $s = L$ .

Interestingly in most cases, the branch or trunk lies in a single plane, so that its shape can be described in 2D (Mouliia & Fournier, 2009). Exceptions are twisted trunks, but their morphogenesis has been studied in less details, but see Zheng *et al.* (2018).

Finally the changes over time of all these quantitative shape descriptors need to be considered, that is  $C(s, t)$ ,  $A(s, t)$ ,  $R(s, t)$  to study morphogenesis and not only a static shape. For example, differential elongation growth can changes curvatures and therefore angles (Fig. 2c,d).

##### 2. Axis spatial display: a tightly controlled process

Botanists studying the architectural development in natural conditions (Halle *et al.*, 1978; Barthelemy & Caraglio, 2007) have paid particular attention to the orientation of the growth axes with respect to the vertical. Orthotropic axes tend toward the vertical, whereas plagiotropic axes remain at a tilted set-point angle. Some axes can be mixed, either plagio-orthotropic or ortho-plagiotropic from base to tip. The orthotropic vs plagiotropic differentiation of axes has been shown to carry over a syndrome of other traits (axis symmetry, apparent phyllotaxis, etc.).

The spatial display of axes is under a continuous active control. Displacing a plant axis from its spontaneous growth direction triggers an active motion powered by its bending motors, either differential elongation in primary growth zones (Fig. 4a,b) or differential shrinkage of reaction wood in secondary growth zones (Fig. 4c). Thanks to live kinematical imaging, the 'choreography' of such active motion has been characterised in a range of species sampling the phylogeny of extant land angiosperms and more than two orders of magnitude in shoot size, at least for the main orthotropic stems (Coutand *et al.*, 2007, 2019; Sierra-De-Grado *et al.*, 2008; Bastien *et al.*, 2013; Gerttula *et al.*, 2015; Okamoto *et al.*, 2015), reviewed in Mouliia *et al.* (2019). All these complex shape-restoring movements show a universal core (Fig. 4d–f). After tilting from its set-point direction, the axis first bends homogeneously, exhibiting a uniform change in curvature and leading to a spatially homogeneous curvature field  $C(s)$ . Soon after, it starts to straighten up from the tip and concentrates its curvature at its base, eventually reaching a typical steady-state shape although the axis is still growing. When submitted to lateral light (on a dark background; Fig. 4g,h) the plant axis also displays a typical movement, first bending towards the light into an almost arc of a circle, until the tip eventually aligns to the light direction. Then it

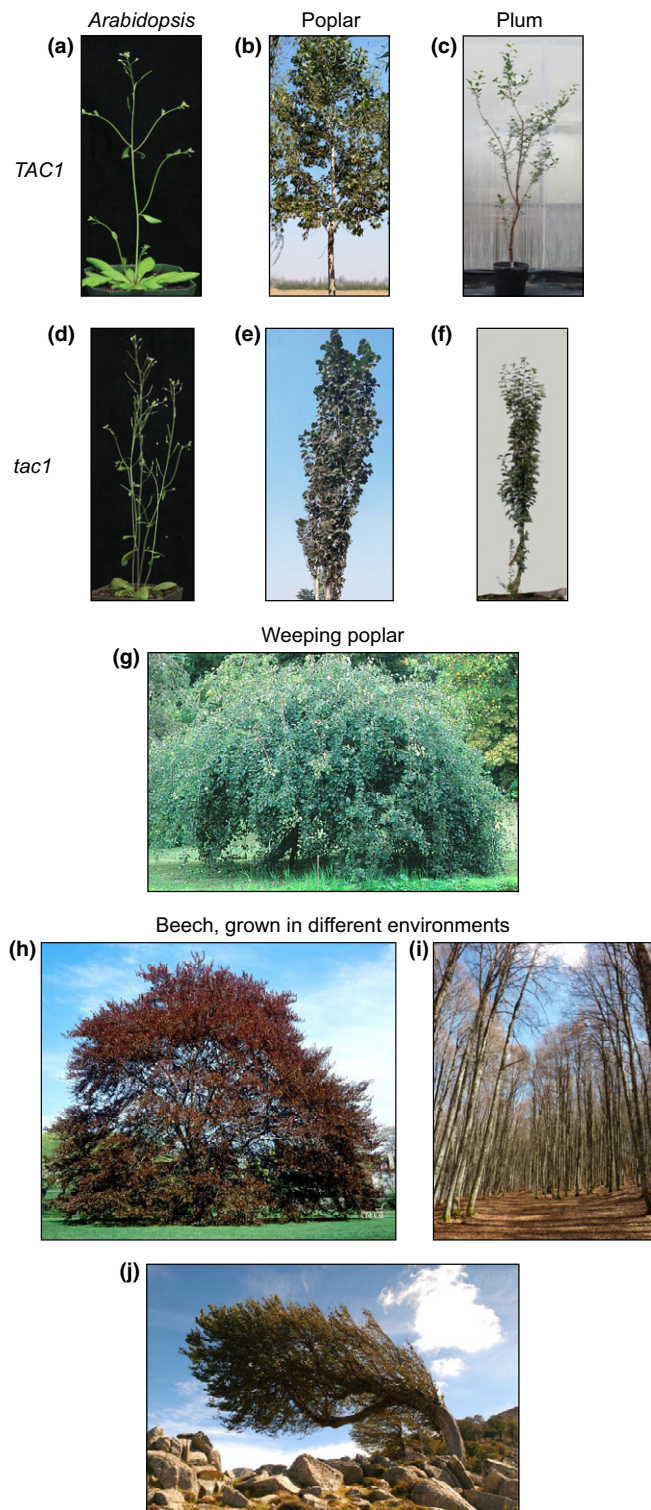


**Fig. 3** Generic genetic and environmental control of crown and axis shapes. (a–g) Genetic control of axis and crown shapes by the *TAC1* and *WEEP* gene families. (a–c) Wild-type forms of the crown in *Arabidopsis thaliana* (a), poplar (*Populus nigra*) (b) and plum tree (*Prunus prunus*) (c). (d–f) Crown shapes in genotypes in which the level of *TAC1* expression has been decreased by knockout artificial mutation (*tac 1* (d)), natural mutation (e) or gene silencing through interfering RNA (f). (g) Weeping poplar, which can be compared with (b) and (e). (h–j) Phenotypic plasticity due to the control of axis development and crown shape by light and wind, illustrated in beech (*Fagus sylvatica*). (h) Beech grown in isolation in a park. (i) Beech in a forest stand. (j) Beech growing on a wind-exposed mountain ridge showing the effect of wind (anemomorphosis) on the crown shape. (a, d) From Waite & Dardick (2018). (b, e) Reproduced from Xu *et al.* (2017) 'PzTAC and PzLAZY from a narrow-crown poplar contribute to regulation of branch angles'. Source: *Plant Physiology and Biochemistry* 2017, 118, 571–578. Copyright © 2017 Elsevier Masson SAS. All rights reserved. (c, f) From Hollender *et al.* (2018a) and Hill & Hollender (2019).

### 3. Unravelling the influence of gravitropic, phototropic and proprioceptive sensing

Plant axes are endowed with two major tropisms: gravitropism and phototropism.

Gravitropism requires a specific sensing apparatus involving gravitropically sensitive cells called statocytes, found all along the stem (Fig. 5a-1; Morita, 2010). Recent studies have shown, through experiments combining live-cell with the kinematical imaging of the whole organ, that statocytes are high-resolution angle sensors (their resolution is *c.* 1°) and not force sensors as previously believed for a long time (Chauvet *et al.*, 2016; Pouliquen *et al.*, 2017; Chauvet *et al.*, 2019; Nakamura *et al.*, 2019).

The mechanism of 'gravicline sensing' (meaning sensing of the inclination angle vs the direction of the gravity) involves avalanches of an intracellular pile of dense amyloplasts (starch grains acting as statoliths), in which the grains are dislodged continuously using active actin–myosin motors so that the pile surface acts as a liquid in the long term and reaches the horizontal (Berut *et al.*, 2018). This movement of the amyloplast piles triggers relocalisation or activation of the auxin efflux transporters PIN3 (Fig. 5a-1), through the involvement of LAZY1 protein. This activation then produces a gradient of auxin (Fig. 5a-2), transmitting the control of the tropic movement to the active bending motors (the expanding cells), according to the classical Cholodny–Went model (see Moulia *et al.*, 2019; Nakamura *et al.*, 2019 for further recent reviews). The *TAC1* protein is also present in the statocytes (Kawamoto *et al.*, 2020) but its cellular role is unknown. Because the statocytes are organised into a sheath of cells that spans all along the shoot (in the endodermis in young stems (Morita, 2010), in the secondary phloem in woody stems; Gerttula *et al.*, 2015), this provides the stem with the ability to sense the inclination angle vs the direction of the gravity *A(s)* all along the stem, and to react at each place through gravitropic bending.

However, it has been demonstrated that this gravicline response is insufficient to drive the shape-restoring movement (Bastien *et al.*, 2013; Dumais, 2013; Okamoto *et al.*, 2015); stems undergo infinite oscillations of decreasing wavelength and amplitude. This is contrary to observations in experiments in which, for all the species

straightens and its tip reaches a steady-state shape with the tip pointing in an intermediate direction between the light direction and gravity (Bastien *et al.*, 2015; Coutand *et al.*, 2019). The question is: 'What controls these universal morphogenetic movements?'

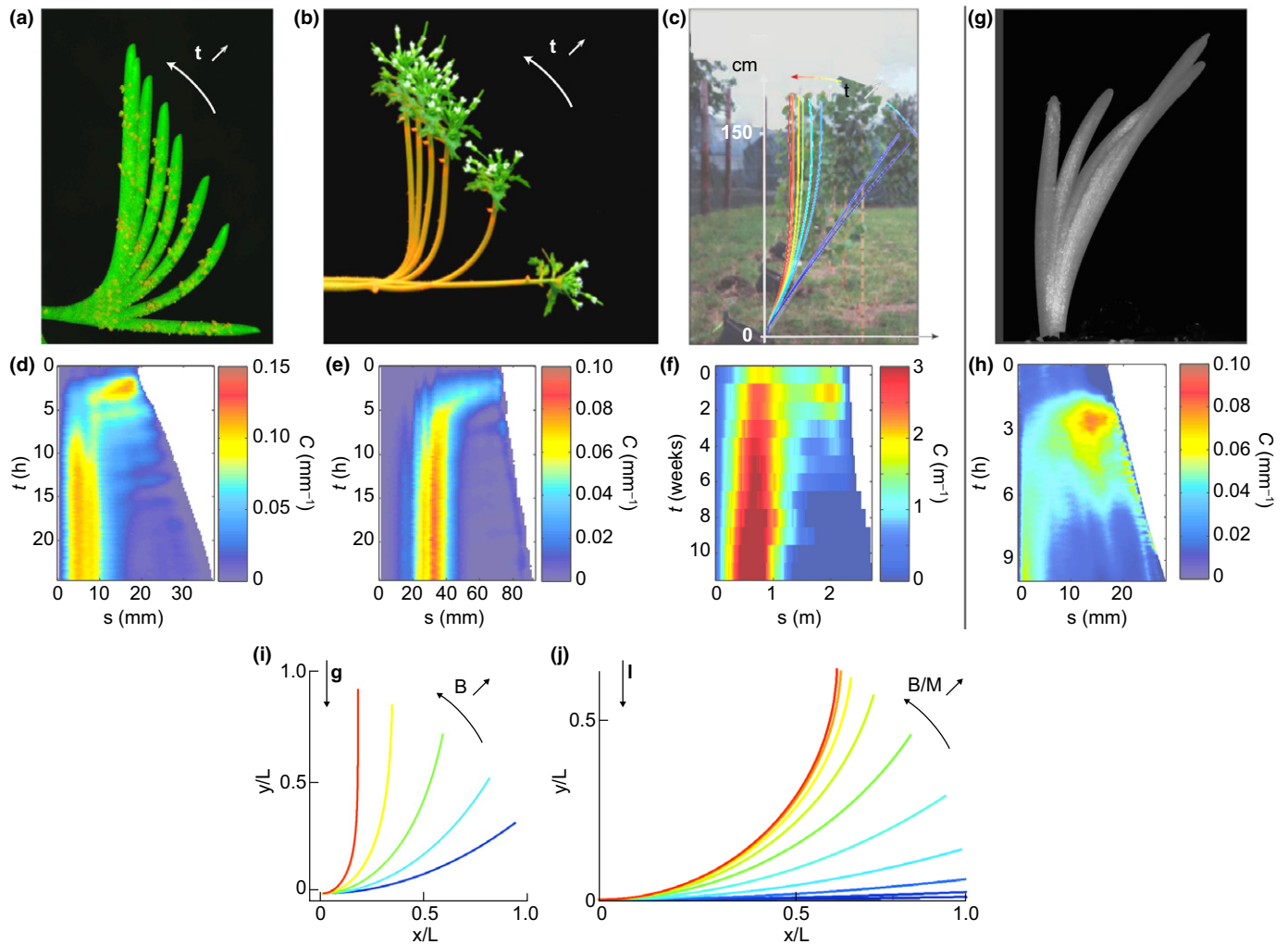
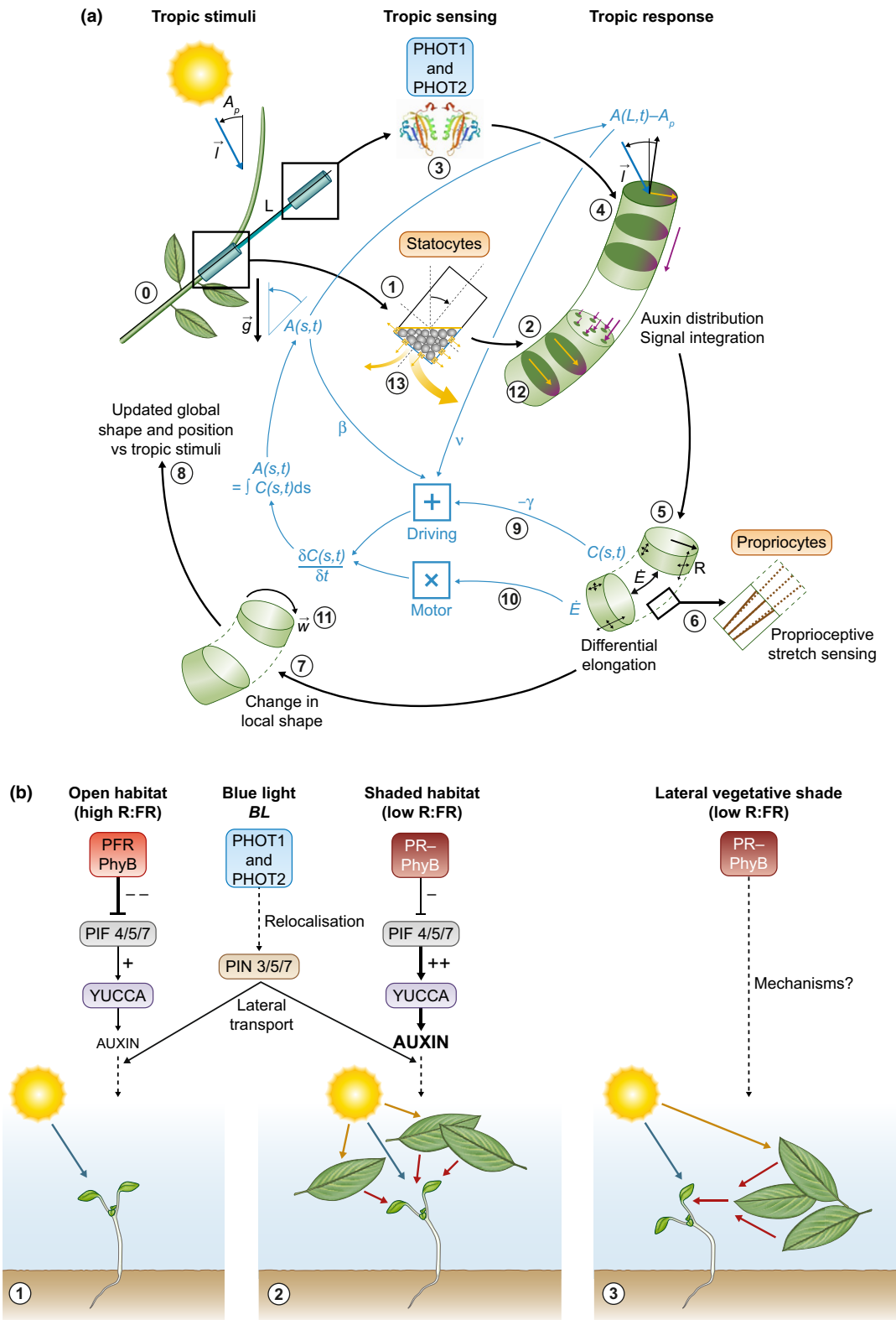


**Fig. 4** The control of tropisms in plant axes. (a–h) Kinematics of the tropic movements of aerial plant organs. (a–f) Gravitropic responses to a tilt to the horizontal. (a) Wheat coleoptile (*Triticum aestivum* L. cv Recital). (b) *Arabidopsis* inflorescence stem (*Arabidopsis thaliana* At L. ecotype Col0). (c) Poplar trunk (*Populus deltoides* × *nigra* cv I4551). Successive shapes of the organs are shown (upper panels) as (a, b) time-lapse photographs or (c) as a graph in the  $x$ – $y$  plane (different colours from blue to red indicate successive shapes, and the dotted blue line indicates the shape of the background photograph). (d–f) Curvature  $C(s, t)$  is mapped as a function of elapsed time after tilting  $t$  and of the curvilinear coordinate  $s$  (the arc length of the central line of the organ as measured from its base). Note the different scales for  $t$ ,  $s$  and  $C$  (colour scale). The tropic movement of all the organs follows a common sequential pattern of global homogeneous curving then downward (basipetal) straightening. (g, h) Phototropic response to a side light in the wheat coleoptile, with  $A_p = -\pi/2$  radians, the angle between the vertical and the light direction. Time-lapse photograph (g) and curvature  $C(s, t)$  map (h). The coleoptile initially curves homogeneously so that its tip tends to align to the light direction, but this bending induces a secondary gravitropic stimulation as pieces of the organ deviates from the vertical ( $A(s, t) > 0$ ). The organ finally aligns to a direction that results from an equilibrium between the phototropic and gravitropic set points, while displaying a downward (basipetal) straightening. (i, j) Steady-state shapes predicted by the model  $A_rC$  presented in the vertical plane in which they lay ( $x$  = horizontal abscissa,  $y$  = vertical abscissa). (i) Steady-state shapes predicted by the model  $A_rC$  with no photoperception (graviproprioceptive drive) as a function of the values of the balance number  $B$ . Lines from green to yellow correspond to  $B = 0.5, 1, 2, 4$  and  $8$ , respectively. (j) Steady-state shape of the  $A_rC$  model with no gravity sensing,  $M \rightarrow 0$  (photoperceptive drive). As  $B/M$  increases, photoperception takes over proprioception (from blue to red); the apical angle reorients in the direction of the light field vector. However, the shape is always an arc of a circle (which is very different from what happens when the distributed graviline sensing is active, see (j)). (a, f) From Moulija *et al.* (2019). (i) From Bastien *et al.* (2013). (g, h, j) From Bastien *et al.* (2015).

tested, the axis tended to a steady-state shape in which curvature tended to concentrate at the base of the axis after undergoing a universal curving–decurving pattern (Fig. 4d–f) (see Moulija *et al.* (2019) for a review). An additional sensing of its own curvature  $C(s, t)$  – or even probably its dimensionless curvature  $\check{C} = C(s, t) R(s, t)$  through proprioception – (Fig. 5a–3) is required for a proper motion control (Bastien *et al.*, 2013, 2014; Moulija *et al.*, 2019, 2021). This has been formalised in the  $AC$  model and validated in many species through: (1)

kinematical experiments (Bastien *et al.*, 2013, 2014; Coutand *et al.*, 2019); and (2) studies of actin and myosin mutants (Okamoto *et al.*, 2015). The putative sensitive cells for proprioception (‘proprioocytes’) may be the young fibre cells that are present just inner to the statocyte sheath; and display actin–myosin cables (Fig. 5a–3) reminiscent of the actin–myosin cables described in mechanosensitive animal cells (Okamoto *et al.*, 2015; Ueda *et al.*, 2015). However, proprioception through mechanosensitive reorientation of microtubules in the



epidermis would also be possible (Muratov & Baulin, 2015) (see Moulia *et al.* (2019) and Moulia *et al.* (2021) for recent and complementary reviews).

The molecular mechanism of phototropic sensing in chlorophyllian angiosperms involves the sensing of gradients in the BL

intensity across the stem axis through the interaction of phototropins 1 and 2 (PHOT1 and PHOT2) (Fankhauser & Christie, 2015; Fig. 5a-4). As light migrates into the interior of a plant stem, it is attenuated by absorption (especially by the chlorophyll for BL) and scattering. The resulting decline in internal BL intensity

**Fig. 5** Dynamics of gravi-phototropic control and schemes of its modelling. (a) Schematic drawing of the cycle of tropic responses followed by plant sensitive to the direction of gravity  $g$  and direction of light  $l$  (with  $A_p$  the angle between  $l$  and the vertical). ① The shoot finds itself at angles with respect to the directions of gravity and light. ② The angle between the axis and the direction of gravity is sensed in specialised cells sitting all along the axis, the statocytes. Upon tilting, the pile of statoliths avalanches to a new position with a roughly horizontal surface. This modifies the distribution of PIN3 auxin efflux transporters (yellow canal) that leads to a dissymmetry in the lateral polar active transport of auxin (yellow arrows), that is proportional to the local angle to the vertical  $A(s,t)$ . ③ This dissymmetry results in a transverse gradient of auxin concentration in every tilted segment of the axis. ④ The internal gradient in blue light in the apical part of the axis is sensed by the interaction between chromo-proteins phototropins 1 and 2 (PHOT1  $\times$  PHOT2); ⑤ this leads to a dissymmetry of the lateral transport of auxin at the apex, which is proportional to the angle of the tip to the light direction  $A(L,t) - A_p$ . The cellular and tissular aspects of this lateral transport are not well established so far. The resulting transverse gradient of auxin concentration at the apex, that is then transmitted downwards by longitudinal polar active auxin transport (purple arrows). ⑥+⑦ Auxin distribution integrates the tropic responses to light and gravity (Cholodny–Went model). ⑧ The difference in auxin concentration between the two sides of the axis drives a differential elongation, which can be viewed as a transverse redistribution of the mean elongation rate  $\dot{E}$  and which tends to modify the local (rest-state) curvature  $C(s,t)$ . ⑨ This differential elongation and/or the curvature  $C(s,t)$  is sensed through the deformation of actin–myosin cables in immature fibre cells, therefore acting as proprioocytes. This drives a feedback response on differential growth, opposing curvature changes. ⑩ The balance between the gravitropic and phototropic drive mediated by auxin, the proprioceptive feedback drive mediated by actin–myosin, and the passive bending under self-weight result in a change in curvature. ⑪ This change in curvature in the segment induces a rotation of all the parts of the stem apical to it. When integrating spatially all the curvature changes, the directions of all the segments along the axis are updated with respect to gravity and light directions. This change in the local angle to the vertical  $A(s,t)$  and the angle of the tip to the light direction  $A(L,t) - A_p$  are again sensed by statocytes and by the PHOT1  $\times$  PHOT2 system and the cycle starts again. After many tropic cycles, the axis reaches a steady-state shape, known as the photo-gravitropic equilibrium, in which the gravi/photo/proprio responses balance each other. Only then the tropic reaction has been achieved and a new posture is seen on the shoot. ⑫ In the  $A,C$  model, the axis shape is driven by three terms: the local angle to the vertical  $A(s,t)$ , the tip angle with respect to the light direction  $A(L,t) - A_p$ , and to the axis curvature  $C(s,t)$ . These three terms are added up, with sensitivities  $\beta, \nu, -\gamma$  respectively, to account for the signal integration through auxin distribution and its interaction with cytoskeleton-mediated proprioceptive responses. This sum drives the rate of change in curvature,  $\partial C(s,t)/\partial t$ , which itself yields an updated global shape with modified  $A(s,t)$  and  $A(L,t) - A_p$  and so on. ⑬ In the  $A,C,\dot{E}$  model, the effect of the mean rate of elongation growth  $\dot{E}(s, t)$  is also included, to account for differences in tropic bending rates due to differences in mean auxin concentration, induced by the genetic background and/or the light environment (see Fig. 5b), or any other source of variation in the mean growth rate; and the curvature  $C(s,t)$  is set dimensionlessly by multiplying it by the radius  $R(s,t)$ ; the sensitivities are rewritten  $\tilde{\beta}, \tilde{\nu}, \tilde{\gamma}$  to specify that they are now independent from the mean rate of elongation growth  $\dot{E}(s, t)$  and from the radius  $R(s,t)$ . ⑭ In the  $AC\dot{E}-\varepsilon_f$  model, the elastic bending under self-weight (due to the bending moment  $W$  that can be calculated in the global geometry of the stem ⑮) is also included (Chelakkot & Mahadevan, 2017). This induces a slack between the actual curvature that is sensed through proprioception  $C(s,t)$  and the rest-state curvature  $C^*(s,t)$ , which is the output of the tropic reactions. ⑯ In their MultiScale Modelling Framework for Tropisms MMFT, Moulton *et al.* (2020) also included explicitly the lateral transport of auxin ⑥+⑦. The lateral transport auxin is still driven by the sensing of local angle to the vertical  $A(s,t)$ , the angle of the tip to the light direction  $A(L,t) - A_p$ , and to its own curvature  $C(s,t)$  (with respective sensitivities  $\beta, \nu, \gamma$  respectively), just as in the  $A,C$  model. However, the integration of these three signals now occurs through a model of auxin lateral transport. In addition Moulton *et al.* (2020) also include the biomechanics of growth (as a plastic irreversible deformations) and the possible 3D display of branches. ⑰ Finally in their position sensor model ( $A_{stat}m$ ), Chauvet *et al.*, 2019 modelled explicitly the biophysics of intracellular statoliths motion leading to gravicline sensing in statocytes ①, while (Levernier *et al.*, 2021) further included the cellular relocalisation of PIN auxin transporters and the building up of the lateral gradient of auxin concentration across the organ. Black arrows, biological and biophysical processes; blue arrows, modelling. Modified from Pouliquen *et al.* (2017) and Moulton *et al.* (2020). (b) Modification of the phototropic responses due to the red/far red (R/FR) light signals mediated by phytochrome (PhyB). ①, ② Goyal *et al.*' qualitative model of the interactions between the major molecular pathways of phototropin-driven phototropism and the phytochrome PhyB sensing. Blue light (BL) gradient acting through phototropin PHOT1 (interacting with PHOT2) is mediated through a dissymmetric auxin lateral transport. In an open environment (high red/far red), active PFR conformation of PhyB inhibits the phytochrome interacting factors (PIFs), thereby leading to reduced *YUCCA* gene expression, resulting in low auxin synthesis. In the shade (low red/far red), the PR conformation of PhyB is inactive and releases PIFs inhibition, leading to high expression of *YUCCA* genes, which itself results in increased auxin levels and promotes phototropism. Note that these effects can be explained by the  $A,C,\dot{E}$  model, through a modulation of the mean rate of elongation  $\dot{E}(s, t)$  due to differences in mean auxin concentration (see panel (a) ⑩). ③ The negative phototropism related to lateral reflection of FR light by neighbouring chlorophyllian organs. This response is mediated by the PR form of PhyB, but its downstream mechanism remains to be studied. ①, ② Modified from Goyal *et al.* (2016).

(fluence rate) is called the BL gradient. However, the BL gradient also strongly depends on the distribution of the light irradiance reaching the stem surface (Vogelmann, 1993). If the stem is more lit from one side compared with from the other, the internal BL gradient is higher than if the stem is lit equally from all its sides (Poff, 1983).

The BL-mediated changes in the PHOT1  $\times$  PHOT2 state drive active bending by building a lateral gradient of auxin concentration (Fankhauser & Christie, 2015; Fig. 5a-5). Surprisingly, the cellular and molecular bases of this lateral gradient auxin are much less known than for gravitropism. This possibly involves (1) the ABCD19 and PIN 3/5/7 auxin influx transporters, as well as an increased synthesis of auxin; and/or (2) an increased auxin diffusion (Fankhauser & Christie, 2015; Goyal *et al.*, 2016). In most species phototropic sensitivity is restricted to the primary growth zone at the tip of the axis (Coutand *et al.*, 2019), so that the phototropic

response depends on the angle between the tip of the axis and the light source (Fig. 5a-5). The built-in auxin concentration gradient that reflects the internal BL gradient in the apical part of the plant is transported down the axis, with little loss through longitudinal active auxin transport (Fig. 5a-5; Moulton *et al.*, 2020). In this way, the axis can bend towards the light direction (sun or canopy opening), until it points in the direction of high light, therefore reducing the differences in irradiance of its faces, and thereby the internal BL gradient. It has been shown, however, that such phototropic sensing alone is not able to drive the orientation: as a unique information (the angle of the tip to the light intensity gradient) is provided to all the positions along axis, it can only bring a spatially constant curvature, that is an arc of the circle, as observed at the beginning of the phototropic reaction (Fig. 4g,h); but it cannot explain the further straightening (Bastien *et al.*, 2015; Moulton *et al.*, 2020).

It should be noted also that PHOT1  $\times$  PHOT2 sensing also interacts with sensing of the red : far red ratio in the lateral and zenithal light through the phytochrome B (PhyB) photosensor (Goyal *et al.*, 2016; Fig. 5b). As red light is almost completely absorbed by chlorophyllian organs (whereas far red light is reflected or transmitted) the red : far red flux ratio provides a neighbouring index (in lateral light; Fig. 5b-3) and a shading index (in the light from above; Fig. 5b-2), two indices that are independent of the global light intensity (Ballare & Pierik, 2017). For low red : far red ratios, phototropism is accelerated (Fig. 5b-2), while it is slowed down in full sunlight (Fig. 5b-1; Goyal *et al.*, 2016). This effect is likely to be mediated by an increased synthesis of auxin in a shaded habitat: this brings a higher mean elongation rate  $\dot{E}$  (Fig. 5a-6) and therefore a faster differential elongation and local bending (Fig. 5a-7). In addition, a direct repulsive effect of a unilateral enrichment in far red light by neighbouring chlorophyllian organs has been described (Fig. 5b-3), but little information is known about its mechanisms (Maddoni *et al.*, 2002).

In natural conditions, gravitropism and phototropism act together to shape the plant axes, but the mechanisms of their crosstalk remain elusive (Coutand *et al.*, 2019; Moulton *et al.*, 2020). A crucial integrative step is obviously the auxin transport (Fig. 5a-2, a-5) and its interplay with cytoskeleton-mediated proprioception (Fig. 5a-6). In addition, as the resulting changes in local shape (Fig. 5a-7) induce large changes in the global orientation of the organ vs gravity and light (Fig. 5a-8), it is important to take into account the whole geometry of the plant and its dynamics until a steady-state equilibrium shape between the different stimuli is reached.

Based on these findings, Bastien *et al.* (2015) have proposed a universal model for the control of the tropic growth of plant axes through the interplay of gravitropic sensing, proprioception and phototropic sensing (limited to the main BL effect so far). This model, called  $A_rC$ , was designed to sense a distant light source such as BL arriving from an unmasked portion of the sky. It has been validated experimentally both on herbaceous light-grown seedlings (Bastien *et al.*, 2015) through the reanalysis of the experiments on the *Avena* coleoptile in the dark by Galland (2002) and on three dicot tree species by Coutand *et al.* (2019) using isotropic light spheres, allowing the separation of gravitropism from phototropism.

The main idea behind the  $A_rC$  model is that active bending at each position on an axis is driven by the sum of three terms: (1) a phototropic term proportional to the difference between the tip angle  $A(L, t)$  and the incident light angle  $A_p$  ( $A_p = 0$  being the vertical light), with a sensitivity  $\nu$ ; (2) a gravitropic term proportional to the angle with the vertical  $A(s, t)$ , with a sensitivity  $\beta$ ; and (3) a proprioceptive term proportional to the curvature  $C(s, t)$ , with a sensitivity  $\gamma$  (Fig. 5a-9). Mathematically the rate of change in curvature  $\frac{\partial C(s, t)}{\partial t}$  can be written as:

$$\frac{\partial C(s, t)}{\partial t} = -\nu(A(L, t) - A_p) - \beta A(s, t) - \gamma C(s, t) \quad \text{Eqn 2}$$

By integrating Eqn 2 over time and space, the whole dynamics of tropic reactions can be simulated numerically and compared with the experiments (Fig. 4a-h); and the dependency of the steady-state shape on the sensitivities can be studied (Fig. 4i,j). However, this requires some preliminary dimensional analysis.

The behaviour of the  $A_rC$  model depends only on two dimensionless numbers, the motion pointing number  $\mathcal{M}$  and the balance number  $\mathcal{B}$ , with

$$\mathcal{M} = \frac{\beta}{\nu}; \quad \mathcal{B} = \frac{\beta L_{gz}}{\gamma} \quad \text{Eqn 3}$$

where  $L_{gz}$  is the length of the reacting growth zone (Fig. 2b).

$\mathcal{M}$  is therefore the ratio between the gravitropic sensitivity and the phototropic sensitivity and sets the photogravitropic set-point angle (PGSA); we will note  $A_r$  as the resultant angle between the gravitropic and phototropic set-point angles.  $A_r$  is found by solving Eqn 2 for the tip angle  $A(L, t)$  when the tip curvature is zero  $C(L, t) = 0$  and consequently  $\frac{\partial C(s, t)}{\partial t}$  is zero too:

$$A_{PGSA} = A_r = \frac{A_p}{1 + \mathcal{M}} \quad \text{Eqn 4}$$

Therefore a large  $\mathcal{M}$ , corresponding to when gravitropic sensitivity  $\beta$  dominates, means that the angle  $A_r$  tends to zero, so that the tip of the axis tends toward the vertical. By contrast, when the gravitropic sensitivity  $\beta$  is negligible and  $\mathcal{M}$  tends to 0, the axis tip is directed towards the light source ( $A(L) \sim A_p$ ).

The balance number  $\mathcal{B}$  is the ratio between the gravitropic sensitivity  $\beta$  and the proprioceptive sensitivity  $\gamma$ , scaled by the growth zone length  $L_{gz}$ . The balance number  $\mathcal{B}$  controls the straightening of the stem and the curvature concentration at the basis of the organ when a steady state is reached (Fig. 4d-g). It also influences the time required for the disturbed axis to reach this steady state (Bastien *et al.*, 2013).

The steady-state shape is reached when  $\frac{\partial C(s, t)}{\partial t}$  is null. Then the solution to Eqn 2 reads:

$$A(s) = \left( A(0) - \frac{A_p}{1 + \mathcal{M}} \right) \left( e^{-\frac{\mathcal{B}s}{L_{gz}}} - e^{-\mathcal{B}} \frac{(1 - e^{-\frac{\mathcal{B}s}{L_{gz}}})}{\mathcal{M} + (1 - e^{-\mathcal{B}})} \right) + \frac{A_p}{1 + \mathcal{M}} \quad \text{Eqn 5}$$

Eqn 5 is particularly complicated, and difficult to interpret as is. However, it is insightful to look at its limit cases. When  $\mathcal{M}$  is very large (i.e. 'pure' gravitropism with negligible phototropic influence, such as for a knockout mutant or isotropic lighting bringing no directional light cue; Coutand *et al.*, 2019), then Eqn 5 simplifies and becomes:

$$A(s) = A(0) \left( e^{-\frac{\mathcal{B}s}{L_{gz}}} \right) \quad \text{Eqn 6}$$

meaning that the angle from the vertical  $A(s)$  decreases exponentially with the relative position along the growth zone of the axis ( $s$ )

$L_{gz}$ ), with a constant relative rate of spatial decay  $\frac{\partial A}{\partial s}$  equal to  $\mathcal{B}$ . The corresponding shapes for different values of the balance number  $\mathcal{B}$  are given in Fig. 4(i). For small  $\mathcal{B}$ , the final form of the axis displays a low curvature and stay very inclined. This can mimic a plagiotropic branch although the gravitropic set-point angle is vertical. For large  $\mathcal{B}$ , the apical part is straight and vertical and the curvature is concentrated at the base (Bastien *et al.*, 2013).  $\frac{\gamma}{\beta}$  controls the length of the curved zone at steady state, which is increased for high proprioceptive sensitivity, and decreased for high gravicline sensitivity. For the tip to be close to the vertical (i.e.  $A(L) < 0.01$  radian  $< 2^\circ$ ), the length of growth zone of the organ should be  $L_{gz} \gtrsim 5 \frac{\gamma}{\beta}$ .

When the gravitropic sensitivity  $\beta$  is negligible (e.g. with a knockout insensitive mutant or during a microgravity experiment), the balance number  $\mathcal{B}$  and the motion pointing number  $\mathcal{M}$  becomes negligible; but their ratio  $\mathcal{B}/\mathcal{M}$  is finite and is equal to the ratio between the phototropic and proprioceptive sensitivities, scaled to the length of the organ  $\frac{\mathcal{B}}{\mathcal{M}} = \frac{\nu L_{gz}}{\gamma}$ . If we further assume that light comes from the vertical zenith ( $A_p = 0$ ), the steady-state shape becomes:

$$A(s) = A(0) \left( 1 - \frac{s}{L_{gz}} \frac{1}{1 + \frac{\mathcal{M}}{\mathcal{B}}} \right) = A(0) \left( 1 - \frac{s}{L_{gz}} \frac{1}{1 + \frac{\gamma}{\nu L_{gz}}} \right) \quad \text{Eqn 7}$$

This displays a spatially constant curvature (therefore the longitudinal shape of the axis is a circular arc; Fig. 4j), the value of which depends on the inverse of  $\mathcal{B}/\mathcal{M}$ . If proprioception dominates over phototropism (i.e.  $\gamma \gg \nu L_{gz}$  and  $\frac{\mathcal{M}}{\mathcal{B}} \gg 1$ ), the axis is straight, with a constant angle  $A(s) = A(0)$  everywhere. By contrast, if phototropism dominates over proprioception (i.e.  $\nu L_{gz} \gg \gamma$  and  $\frac{\mathcal{M}}{\mathcal{B}} \ll 1$ ), the axis curves until the tip angle  $A(L)$  tends to 0, so that the tip tends to align with the direction of light (here the vertical).

Finally, when both the phototropism and gravitropism are active, the steady shape depends on  $\mathcal{B}$  and  $\mathcal{M}$ , and on the two boundary conditions, that is the direction of light  $A_p$  and the insertion angle  $A(0)$ . If the light comes from above  $A_p = 0$  (as with an isolated stem in a standard growth chamber) then the tip points at the PGSA, which is vertical. In case of conflict between gravitropism and phototropism, such as for example for a basal branch shaded by the above-crown, the set-point angle is given by Eqn 4.

A last element to consider is how the phototropic sensitivity  $\nu$  and the gravitropic sensitivity  $\beta$  may depend on the light conditions. This topic now becomes better understood (Fankhauser & Christie, 2015; Goyal *et al.*, 2016). For chlorophyllous light-grown stems, the photosensitivity  $\nu$  depends on the intensity of the directional BL flux density through the interaction between PHOT1 and PHOT2 proteins (Fig. 5b). To quantify this response of  $\nu$  to BL,  $\nu(\text{BL})$ , one can fit the value of  $\mathcal{M}$  in the  $A, C\dot{E}$  model to experimental data under different light conditions. Doing so, a power-law dependency between  $\mathcal{M}$  and BL was found (Bastien *et al.*, 2015; Coutand *et al.*, 2019). As expected the parameters of this response of  $\mathcal{M}$  to BL,  $\mathcal{M}(\text{BL})$ , are species dependent (Coutand *et al.*, 2019). Whether this involves only a

dependency of  $\nu$  or if the light conditions may affect  $\beta$  also is a matter of debate. As stated before,  $\mathcal{M}$  may also depend on the red : far red light background (Fig. 5b) but this has not been modelled yet.

Note, finally, that when considering the bending of the primary growth zone, it is even possible to extract the effect of the mean relative elongation rate of the organ  $\dot{E}$  on the rate of the bending response as defined by Eqn 2 (Fig. 5a-10; Bastien *et al.*, 2014; Pouliquen *et al.*, 2017; Moulia *et al.*, 2019), leading to the  $A, C\dot{E}$  model:

$$\begin{aligned} \frac{DC(s, t) \cdot R}{Dt} &= \dot{E}(-\nu(A(L, t) - A_p) - \tilde{\beta}A(s, t) - \tilde{\gamma}C(s, t) \cdot R) \\ &= \dot{E} \left( -\frac{\nu R}{E}(A(L, t) - A_p) - \frac{\beta R}{E}A(s, t) - \frac{\gamma}{E}C(s, t)R \right) \end{aligned} \quad \text{Eqn 8}$$

where  $D/Dt$  is the derivative following every segment of the stem within the growth zone (as their position along the growth zone may change with growth).

The interest of Eqn 8 is to split the effect of the driving sensitivities from that of the mean growth rate. Therefore there is no confusion between (1) tilt-sensitive plants; and (2) fast-growing and therefore fast-reacting plants (the latter either due to genetic differences and/or to environmental effects on auxin – or other hormone – synthesis, linked for example to the red : far red ratio of the light; Fig. 5b). Moreover, it is dimensionless, taking into account a second relevant intrinsic size scale (the mean radius  $R$  of the growth zone), and a relevant intrinsic time scale, the time for doubling length through elongation growth  $\tau_g = \frac{1}{\dot{E}}$ . In the  $A, C\dot{E}$  model:

$$\mathcal{M} \text{ is unchanged } \mathcal{M} = \frac{\tilde{\beta}}{\tilde{\nu}} = \frac{\beta}{\nu} \text{ but } \mathcal{B} \text{ now comes as } \mathcal{B} = \frac{\tilde{\beta} L_{gz}}{\tilde{\gamma} R} \quad \text{Eqn 9}$$

Therefore, once the effect of growth rate has been separated from that of the pure differential driving of the tropic response,  $\mathcal{B}$  no longer depends on the size of the growth zone, but only on its aspect ratio  $\frac{L_{gz}}{R}$  (its slenderness), that is on a shape characteristics.  $\mathcal{M}$  and  $\mathcal{B}$  are therefore intensive parameters; they do not depend on the size or the volume of the plant, but on its tropic sensitivities and, through  $\mathcal{B}$ , on the slenderness of the growth zone (Moulia *et al.*, 2019).

So far, we have studied vertical stems that have eventually been tilted and that actively react and reach a steady PGSA, note  $A_p$ , with a proprioceptive-driven straightening constraint. Can this approach be insightful to understand the shaping of lateral branches?

#### 4. Lateral vs main shoots? What does it change?

**Bud angles or lateral set-point angle?** The control of the spatial display and shape of lateral branches have been studied actively over the last few years. The initial condition for the new lateral branch is

the axillary bud angle (Fig. 1d). This angle varies between species and is under hormonal control (Williams & Billingsley, 1970). However, the development of branch shape is mostly controlled through active bending of the growing stem driven to a steady set-point shape by external and internal cues (Fig. 5a), just as in the main shoot (Roychoudhry & Kepinski, 2015; Hill & Hollender, 2019). This has been shown in elongating part of the axes (Roychoudhry *et al.*, 2013, 2017), and also in the woody part of the axis, where reaction wood provides a footprint of the active bending that have been involved to control curvature changes over time (Fig. 6a,b; Fisher, 1985; Yamamoto *et al.*, 2002; Gerttula *et al.*, 2015; Hung *et al.*, 2017).

In the context of lateral branches, a popular concept is the gravitropic set-point angle (GSA), initially defined by Digby & Firn (1995) and brought up to date recently (Roychoudhry & Kepinski, 2015). The GSA (noted as  $A_{GSA}$  in the following), is the angle with respect to gravity at which an organ is maintained through active gravitropic movement. A vertical orthotropic axis has a GSA of  $A_{GSA} = 0$  from the vertical. A plagiotropic horizontal axis has a GSA of  $A_{GSA} = \pi/2$  radians. The GSA can be revealed through a reorientation test (in conditions in which phototropism is negligible, Coutand *et al.*, 2019): an axis growing at a steady angle is tilted. If it goes back to its initial angle, this angle approximates its GSA (Roychoudhry & Kepinski, 2015).

Including the GSA into the  $A, C$  model yields:

$$\frac{\partial C(s, t)}{\partial t} = -\nu(A(L, t) - A_p) - [\beta(A(s, t) - A_{GSA})] - \gamma C(s, t) \quad \text{Eqn 10}$$

In this case, the PGSA  $A_{PGSA}$  becomes:

$$A_{PGSA}(L, \infty) = \frac{\nu A_p + \beta A_{GSA}}{\nu + \beta} = \frac{A_p + \mathcal{M} \cdot A_{GSA}}{1 + \mathcal{M}} \quad \text{Eqn 11}$$

This means that the set-point angle that is observed in a real plant (e.g. in a real tree crown), where phototropism and gravitropism take place, is a mixture of  $A_p$  and  $A_{GSA}$ , which is tuned by the motion pointing gravitropic/phototropic number  $\mathcal{M}$ .

**Molecular mechanisms controlling the set-point angle of lateral branches** The cellular and molecular mechanisms leading to a GSA different from 0 are not obvious. They should share a common core with the cellular mechanisms established for ortho-gravitropic main axes. Indeed, it is well known that, in many species, the removal of apical dominance can shift a plagiotropic axis with large GSA into an orthotropic axis with zero GSA (Roychoudhry & Kepinski, 2015). However, defining what has been switched through the removal of apical dominance remains an open question. Considering the statocytes, there should be an offset in the way that the (horizontal) pile of statoliths influences PIN auxin efflux transporters. Within the position sensor model PSM of Pouliquen *et al.* (2017) (Fig. 5a-10), a modulation of the GSA could be achieved by

shifting the activity/density of PIN transporters in the basal membrane of the statocytes.

Roychoudhry *et al.* (2013) proposed another model: the antigravitropic offset model (AGO), which is receiving increasing experimental support by Kawamoto *et al.* (2020). They showed that when lateral branches of Arabidopsis are continuously clinorotated (to prevent the gravitropic sensing), they display extensive outward curvature (Fig. 6c,d). The magnitude of this effect is specified by the total amount of auxin in the axis. To account for these observations Roychoudhry *et al.* (2013) proposed the qualitative model (Fig. 6g), in which a constant efflux of auxin occurs from the side of the statocyte opposite to the position of the settled statoliths. When alone, this mechanism led to a homogeneously curved axis (i.e. an arc of circle).

Kawamoto *et al.* (2020) used the triple *lazy* knockout mutant *lz1,2,3* to investigate the AGO mechanisms by comparing it with wild-type *Arabidopsis thaliana* (WT). The triple *lazy* knockout mutant *lz1 1;2;3* (in which three genes from the *LAZY* family were inactivated) has normal gravisensitive statocytes but lacks gravitropic orientation because it cannot set a lateral gradient in auxin allowing for differential growth (Yoshihara & Spalding, 2017). Kawamoto *et al.* (2020) found that, while the lateral branches in the WT were positively gravitropic, the *lz1 1;2;3* globally displayed a horizontal habit, but with a slight curving (with an abaxial concavity), that may reveal an AGO mechanism. Then they studied the effect on the lateral branches of upside down turning of the plant. They found that the WT lateral branches reoriented rapidly upwards (gravitropic reaction; Fig. 6e) whereas in the mutant *lz1 1;2;3* they bend downwards (and therefore displayed an adaxial concavity; Fig. 6f). This definitively demonstrated that AGO is independent of the *LAZY* pathway.

We still lack a great deal of details on the molecular and cellular mechanisms of AGO. However, we may assess if it is able to explain quantitatively the shaping of lateral branches, and how it may interact with graviceptive, photoceptive and proprioceptive controls.

Restating the AGO qualitative model into the  $A, C$  quantitative model yields:

$$\frac{\partial C(s, t)}{\partial t} = -\nu(A(L, t) - A_p) - \beta(A(s, t)) + \kappa_{AGO} - \gamma C(s, t) \quad \text{Eqn 12}$$

where  $\kappa_{AGO}$  represents the constant rate of curvature resulting from the active efflux towards the antigravitropic part of the lateral axis. We may call Eqn 12 the  $A, C_r$  model (for a reason to be explained later on). Note that the sign of  $\kappa_{AGO}$ , depends on the angle between the parent shoot and the vertical: if the parent shoot is directed upwards then  $\kappa_{AGO} > 0$  meaning that the concavity is abaxial (Fig. 6d). If the parent shoot is directed downwards (Fig. 6e) then  $\kappa_{AGO} < 0$  meaning that the concavity is adaxial. For a seminal stem with no parent shoot,  $\kappa_{AGO} = 0$ .

This situation with a constant source of curvature  $\kappa_{AGO}$  shares similarities with the one studied by Bastien *et al.* (2015), and we

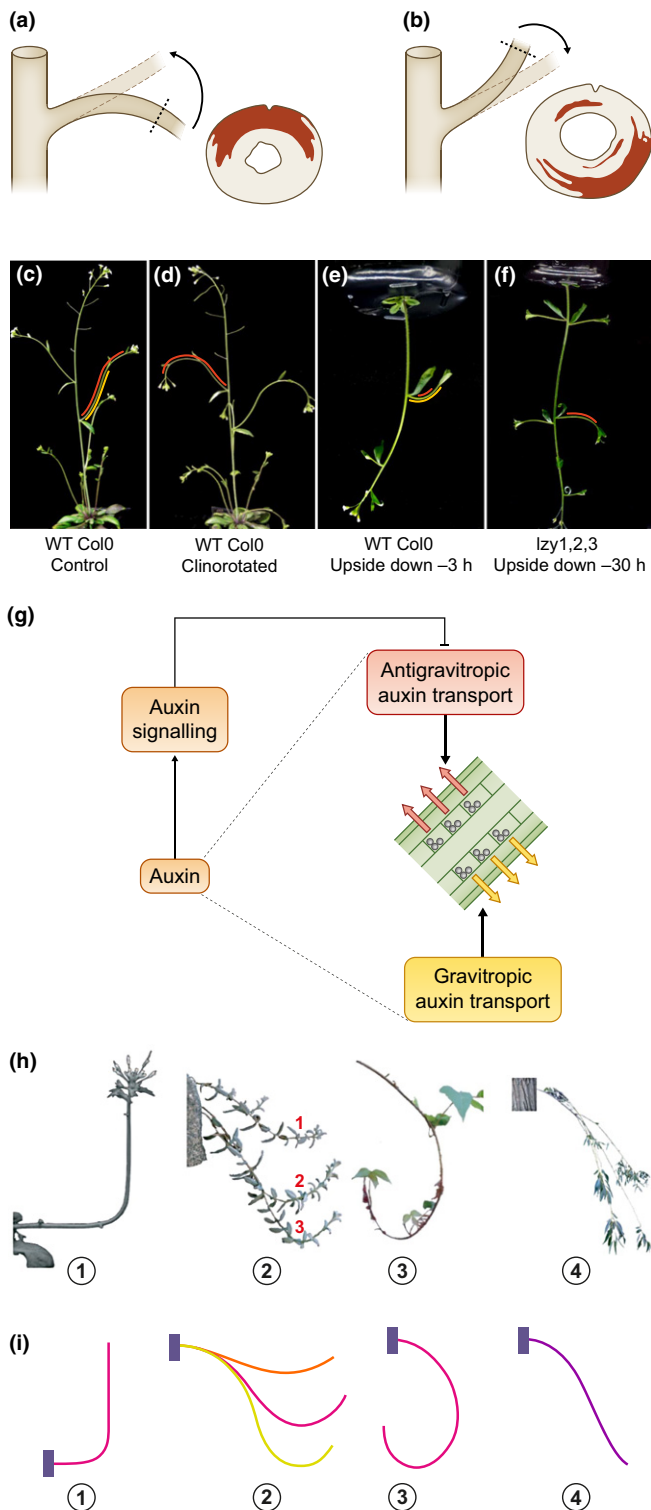


**Fig. 6** Shape control in lateral axes. (a, b) Distribution of tension wood in a lateral branch of *Terminalia catappa*, which has been artificially bent up and tied, or bent down and tied. The tension wood is shown as brown areas in the cross-sections. It acts on the active bending through its high longitudinal shrinkage. The tension wood is set so to correct for the disturbance, and to bring the axis back to its tropic set-point angle. (c, d) Lateral branch shape in a wild-type *Arabidopsis thaliana* (cv Col0) when grown under normal earth conditions (c) or on a clinostat (d) that nullifies the gravicline sensing. Nullifying gravicline sensing brings a clear and homogeneous curving of the growth zone. (e, f) Lateral branch shape in wild-type (WT) and the *lzy1;2;3* triple mutant deprived of gravicline sensitivity when the plant is grown upside down. In the wild-type the lateral axis undergoes gravitropic bending up (e). In the *lzy1;2;3* triple mutant the actively growing lateral branches (red and yellow lines) clearly bend in the opposite direction (f). Note that, when comparing (d) and (f), it is obvious that the active bending observed upon the release of gravitropic control can be abaxial or adaxial; this demonstrates that this is not an epinastic but an antigravitropic offset active bending. (g) Schematic model of the action of the auxin-dependent gravitropic and antigravitropic offset components showing regulation of the antigravitropic offset by auxin that occurs within the gravity-sensing cells. Yellow and red arrows represent the gravitropic and antigravitropic auxin transport components, respectively. (h) Effect of elastic sagging on the control: typical examples of the range of shapes of shoots and branches with increasing effects of elastic sagging during their growth. ① *Arabidopsis* inflorescence stem; ② *Cerastium tomentosum* L. shoots of three different lengths; ③ *Toxicodendron radicans* L. shoots displaying curvature reversal; ④ small *Salix alba* L. branches. (i) Different predictions (①–④) of the ACÉ-εI model showing that it can mimic the real shapes in (h). (a, b) Redrawn from Fisher (1985). (c, d, g) Modified from Roychoudhry *et al.* (2013). (e, f) Modified from Kawamoto *et al.* (2020). (h, i) Modified from Chelakkot & Mahadevan (2017).

$$A_{PGSA}(L, \infty) = \frac{\nu A_p + \kappa_{AGO}}{\nu + \beta} = \frac{A_p + \frac{1}{\nu} \kappa_{AGO}}{1 + M} \quad \text{Eqn 13}$$

Interestingly, although expressed as an antigravitropic curvature rate  $\kappa_{AGO}$ , this model results in an apparent offset of the PGSA at the tip of the axis. This can be clearly seen by equalising Eqns 10 and 12, showing that the apparent set-point angle observed in conditions of no phototropism (Coutand *et al.*, 2019), and interpreted as a GSA, becomes:

$$A_{GSA_{app}}(L, \infty) = \frac{\kappa_{AGO}}{\beta} \quad \text{Eqn 14}$$

Note that this apparent GSA ( $GSA_{app}$ ), and therefore strictly speaking the antigravitropic offset, are not set directly by  $\kappa_{AGO}$  (and therefore by the amount of antigravitropic auxin efflux) but by its ratio with the gravitropic sensitivity  $\beta$ . This has implications for the studies of the relationship between the AGO phenotype of lateral axes and the underlying cellular mechanisms.

Eqn 12 of the  $A_r C_r$  model brings another insight. Indeed, if we study the case of an atropic mutant ( $\beta = 0, \nu = 0$ ) or a clinostated plant in the dark (or in isotropic lighting), the steady state of the axis is uniformly curved, with a resultant constant curvature  $C_r$  given by:

$$C(s) = \frac{\kappa_{AGO}}{\gamma} = C_r \quad \text{Eqn 15}$$

This fits with the experimental reports on clinostated plants in darkness by Roychoudhry *et al.* (2013) (Fig. 6c,d), and can be

can speculate that the gravitropic curving rate  $\kappa_{AGO}$  can be balanced by the proprioceptive control.

In this case, by comparing the PGSA  $A_{PGSA}$ , in the standard case of an upwards parent stem (Fig. 6d); Eqn 12 becomes (with  $C(s, t) = 0$  and  $\frac{\partial C(s, t)}{\partial t} = 0$ ):

viewed as a set-point curvature  $C_{SP} = C_r$  (Meroz & Silk, 2020). This view of a set-point curvature in lateral axis, leading to active weeping, is actually more straightforward than that of a set-point angle, given the mechanism of auxin antigravitropic efflux.

Then a third dimensionless number, that we will call the (active) weeping number  $\mathcal{W}$ , can be defined:

$$\mathcal{W} = \frac{\kappa_{AGO} R}{\gamma} \quad \text{Eqn 16}$$

where  $R$  is the typical diameter of the growing axis undergoing active weeping.

$\mathcal{W}$  indicates that the weeping phenotype is driven by the ratio between  $\kappa_{AGO}$  and  $\gamma$ : for example a straight habit can result either from a low antigravitropic curving rate  $\kappa_{AGO}$  or from a high proprioceptive sensitivity  $\gamma$ .  $\mathcal{W}$  also indicates that the radius  $R$  of the lateral axis matters: the  $\kappa_{AGO}/\gamma$  ratio should scale to this radius to bring a similar shape irrespective of size.

It would be too speculative to go beyond this point in this review. Nevertheless, the above paragraphs illustrate how experimental physiological results and formal modelling can crosstalk to better understand shape control. Indeed, a formal model can be an efficient way to collate the literature, bringing new insights, such as the antagonistic interplay between AGO and the proprioceptive driving. Additionally it may be used to quantitatively estimate the value of the control parameters in wild-type and mutant lines, and may help to design the relevant experiments (Coutand *et al.*, 2019).

**Adding elastic sagging and growth** The  $A_rC$  model does not explicitly take into account elastic sagging under self-weight (Chelakkot & Mahadevan, 2017). Briefly (as a recent review is available on this topic; Mouliia *et al.*, 2019; Meroz & Silk, 2020), elastic sagging is significant in twigs and slender shoot that can display passive weeping (Fig. 6h-4). This has the important consequence that the actual curvature  $C(s,t)$  differs from the rest-state curvature  $C^*(s,t)$  produced by differential growth, this difference is due to elastic bending. As only the actual curvature  $C(s,t)$  can be sensed through proprioception, whereas the output of tropic control is the rest-state curvature  $C^*(s,t)$ , shape regulation is more complex than in the  $ArC$  model (Chelakkot & Mahadevan, 2017; Moulton *et al.*, 2020). The elastic passive bending depends on the distribution of weights along the axis; but also on the amplifying effect of the corresponding lever arms, such that longer axes should bend more (Mouliia *et al.*, 1994). This is resisted by the flexural rigidity ( $F_r$ ) of the axis that depends on the stiffness of the constitutive tissues (Young's modulus), and also on the 4<sup>th</sup> power of the diameter. Therefore, this bending stiffness varies strongly along a tapered axis (Mouliia *et al.*, 1994).

To handle all this Chelakkot & Mahadevan (2017) combined the *elastica* theory of large elastic bending under self-weight (torque balance equation) with the  $ArC$  model, leading to what was later called the  $ACE-\mathcal{E}_l$  model (Mouliia *et al.*, 2019). This model takes both the longitudinal growth rate  $\dot{E}$  and the elastic bending into account, although with only the graviproprioceptive drive (no phototropism). From the torque balance, it was found that the amount of passive bending under self-weight was driven by the dimensionless 'elastic sagging number'  $\mathcal{E}_l$ :

$$\mathcal{E}_l = \frac{L_{gz}}{\left(\frac{F_r}{\rho g}\right)^{\frac{1}{3}}} \quad \text{Eqn 17}$$

where  $F_r$  is the flexural rigidity,  $L_{gz}$  the length of the growth zone, and  $\rho g$  is the weight per unit length. Within this new model, the shape of the shoots depends both on the active tropism and on elastic sagging (Figs 5a-11, 6i). Then Moulton *et al.* (2020) in their MultiScale Modelling Framework for Tropisms (*MMFT*) also included the biomechanics of growth (as a plastic irreversible deformations) and the possible 3D display of branches (as well as the explicit lateral transport of auxin triggering differential growth; Fig. 5a-12); but have not yet yield characteristic additional dimensionless numbers. In addition, note that the active antigravitropic curving controlled by the weeping number  $\mathcal{W}$  has not yet been incorporated into the  $ACE-\mathcal{E}_l$  and *MMFT* models. So the difference between active weeping and passive sagging is not implemented, although active weeping lateral organs are many in nature (Mouliia *et al.*, 1994; Tadrict & Darbois-Textier, 2016; Hollender *et al.*, 2018a).

For axes undergoing both primary and secondary growth, elasticity plays an even more complex role. Indeed the inner core of previously formed wood resists active bending, while the new peripheral layers of wood are involved in active bending through reaction wood formation and maturation shrinkages (Mouliia & Fournier, 2009). Depending on the relative dynamics of primary growth vs secondary growth, branches may, or may never, reach a steady shape (Almeras *et al.*, 2002; Almeras & Fournier, 2009). However, in most cases, the lateral axis reaches its steady-state shape defined by photoceptive, graviceptive and proprioceptive drive.

Finally, one may wonder if an axis is able to control its amount of elastic sagging. More than 40 yr ago, McMahan & Kronauer (1976) proposed that tapering of plagiotropic lateral branches may have been optimised mechanically during evolution to reach a state called 'elastic similarity'. This state provides the maximum possible horizontal span for a branch of a given branch volume, and allometric tapering and a rest-state curvature  $C^*(s,t) = 0$  (Fig. 2a). Indeed increasing the length would make the branch sag more and more until the horizontal span would eventually decrease rather than increase. However, this provided no clues on the underlying morphogenetic process. Moreover, it comes now as an outdated view, as it fully neglected the active control of axis spatial display detailed previously (Mouliia & Fournier, 1997, 2009). However, even if the 'elastic similarity model' is obsolete, the idea that the mechanical effect of self-weight (amplified by lever arms) may be sensed by the organ and drives its growth in diameter and/or eventually in length to control its  $\mathcal{E}_l$  may still hold. Indeed, it is well known that externally applied bending drives growth responses called thigmomorphogenesis that reduce longitudinal growth and stimulate radial secondary growth (when a cambium is present), as reviewed in Chehab *et al.* (2009) and Mouliia *et al.* (2015). This is clearly established for the response to wind-induced bending. Now, what about bending under self-weight? We have seen that axes are able to sense their curvature through proprioception. However, the thigmomorphogenetic effect of self-weight has only been studied for orthotropic main stems (Ko *et al.*, 2004; Alonso-Serra *et al.*,

2020). Moreover, coming back to lateral branches it is not clear whether the branch is dimensioned to cope mainly with wind loads or to its self-weight. In addition, even if such self-weight control exists, it may present a trade-off between minimising  $\mathcal{E}_l$  and minimising the breaking risk (under its own weight or, more probably, under wind loads, that induce much higher mechanical stresses and hazards; Eloy *et al.*, 2017).

**Models as integrative tools for axis systems biology** We have seen that models are required to handle the feedback cycle between local cellular processes (sensing and differential growth) and the updated global shape and position feeding back on the next step of the tropic movement (Fig. 5a). Thereby they formalise the dynamic link between local control mechanisms (including gene products such as the LAZY family, TAC1 or WEEP) and the global phenotype of the axis shape. All the models reviewed so far ( $A_rC$ ,  $A_rC\dot{E}$ ,  $A_rC_r$ ,  $AC\dot{E}-\mathcal{E}_l$  and  $MMFT$ ), as successive development of the  $A_rC$  core model, share this essential feature that allows the gap to be bridged between molecular/cellular biology and whole plant shaping. These models can, however, be distinguished by three criteria: (1) their scale span; (2) their way of considering growth; and (3) the fact that they can lead to closed-form formulae (as for example for the steady-state shape of the  $A_rC$  and  $A_rC_r$  models) or only to numerical simulations. The scale span of the  $A_rC$ ,  $A_rC\dot{E}$ ,  $A_rC_r$ ,  $AC\dot{E}-\mathcal{E}_l$  and  $MMFT$  models is from an element of tissue to the cross-section and then to the whole plant axis. The sensing mechanisms (gravisensing, photosensing and proprioception) involve state variables at the level of a small 'slice' of the organ (angle  $A(s,t)$  and curvature  $C(s,t)$ ; Fig. 5a). Only the position sensor model by Pouliquen *et al.* (2017); Berut *et al.* (2018) and Chauvet *et al.* (2019) details the behaviour of a sensitive cell (the statocyte; Fig. 5a-12). The way to handle growth and its link with the sensing mechanisms may also differ. Kinematical models  $A_rC$ ,  $A_rC\dot{E}$ ,  $A_rC_r$  only consider expansion and bending growth rate of each organ slice that are driven by the sensed variables; whereas, as biomechanical models,  $AC\dot{E}-\mathcal{E}_l$  and  $MMFT$  consider the forces due to growth and to self-weight.  $MMFT$  also specifies the link between angle sensing and the transport of auxin in the tissues. Finally, only  $A_rC$  and  $A_rC_r$  can be solved analytically to close-form formula to at least their steady-state shapes, revealing controlling dimensionless numbers controlling the shape of the axis.

**The dimensionless numbers of axis morphogenesis: the  $\mathcal{BM}_W\mathcal{E}_l$  morphospace and its possible genetic control** The  $A_rC$  model family shows that axis morphogenesis is driven from its initial angle  $A(0)$  with respect to two absolute external references: the gravity vector and the light-gradient vector (when anisotropic). Importantly, this drive also involves two internal references: the GSA  $A_{GSA}$  (Roychoudhry & Kepinski, 2015) and the set-point curvature  $C_{SP}$  (Meroz & Silk, 2020). In an orthotropic and straightening axis,  $A_{GSA} = 0$  and  $C_{SP} = 0$  too. In lateral axes, the GSA and the set-point curvature may be zero, and their apparent value in experiments comes, respectively as a balance between the antigravitropic curvature rate and gravicline sensing  $A_{GSA-app}(L, \infty) = \frac{\kappa_{AGO}}{\beta}$  or proprioceptive sensing  $C_{SP-app} = \frac{\kappa_{AGO}}{\gamma}$ .

Moreover, the way the axis shapes according to the four references depends on its relative sensitivities toward (1) the gravity direction, (2) the light gradient and (3) its own curvature. This is captured by two major dimensionless numbers: the balance number  $\mathcal{B}$  and the motion pointing number  $\mathcal{M}$ . In lateral axes, when an antigravitropic offset curving rate is included, the dimensionless weeping number  $\mathcal{W}$  needs to be added. Together they define a continuous 3D *morphospace*, defining all the possible steady-state shapes that an axis can reach. As only the effects of  $\mathcal{B}$  and  $\mathcal{M}$  control have been validated and published, we first present the  $\mathcal{BM}$  morphospace within the universal  $A_rC$  model, as illustrated in Fig. 7(a,b). In this figure the steady-state shapes are shown for an axis with orthotropic ( $A_{GSA} = 0$ ) and straight ( $C_{SP} = 0$ ) set points and no AGO, starting its growth with an initial angle  $A_0 = -\pi/2$  radian (e.g. a lateral branch). Two cases of lighting are illustrated: a case with a typical direct summer sunlight  $A_p = \pi/3$  radian (Fig. 7a); and a case with the light reflected from below at  $A_p = 2\pi/3$  radian, as approximately found for a branch sitting below a canopy and extending over a lake that reflects the sunlight (Fig. 7b).

For  $\mathcal{B}$  close to zero the proprioceptive straightening dominates gravitropic bending and the axis keeps it in a horizontal direction (except if phototropism takes over proprioception, according to the value of  $\frac{\mathcal{B}}{\mathcal{M}} = \frac{\nu_{\mathcal{E}_l}}{\gamma}$ , in which case the axis shapes into an arc of circle). Let us now consider the situation at high  $\mathcal{M}$  (gravicline sensing taking over phototropic sensing). As  $\mathcal{B}$  increases, the axis tends more towards the vertical and concentrates spatially its curvature at the base of the axis (as observed experimentally; Fig. 4d-f). Decreasing the motion pointing number  $\mathcal{M}$  so that phototropic driving increases its share, leads to a photogravitropic equilibrium for the resultant angle  $A_r$  at the tip. This tip angle tends towards the light direction as  $\mathcal{M}$  reaches very low values. However, the length of the curved zone  $L_c$  depends only on the balance number  $\mathcal{B}$ ; so that at higher  $\mathcal{B}$  the apical part of the stem becomes straighter, clearly pointing at the PGSA  $A_r$  (as observed experimentally; Fig. 4g,h). Note that, because the axis has a finite length and his curvature is restrained by proprioception, the tip angle may not reach its  $A_r$ , especially for low balance numbers  $\mathcal{B}$ . This suggests that care should then be taken when assuming that steady-state tip angles reflect directly the set-point angle (for example the GSA). Altogether, Fig. 7(a) clearly illustrates the large amount of plasticity provided by the  $\mathcal{BM}$  control, in a standard situation of an isolated axis. This is even more dramatically illustrated for lighting from below (Fig. 7b). Although the axis has a vertical GSA it may actively bend downwards as  $\mathcal{M}$  reaches low values.

The effect of passive elastic sagging can be studied by considering the morphospace for the balance number  $\mathcal{B}$  vs the passive elastic sagging number  $\mathcal{E}_l$  in the frame of  $AC\dot{E}-\mathcal{E}_l$  (Chelakkot & Mahadevan, 2017) (i.e. at very large  $\mathcal{M}$ ; Fig. 7c). When  $\mathcal{E}_l$  is high, the shoot sags much more and the shape can be almost overwhelmed by the sagging. An interesting situation is for intermediate  $\mathcal{E}_l$ , in which, depending on  $\mathcal{B}$ , the axis can either bend downwards, displaying a mixture of plagiotropism and orthotropism, or even become orthotropic and point towards the vertical at high  $\mathcal{B}$ . Altogether, these observations show that the internal control of shape in plant axes summarises to only three traits, the  $\mathcal{BM}_W\mathcal{E}_l$  triplet, or

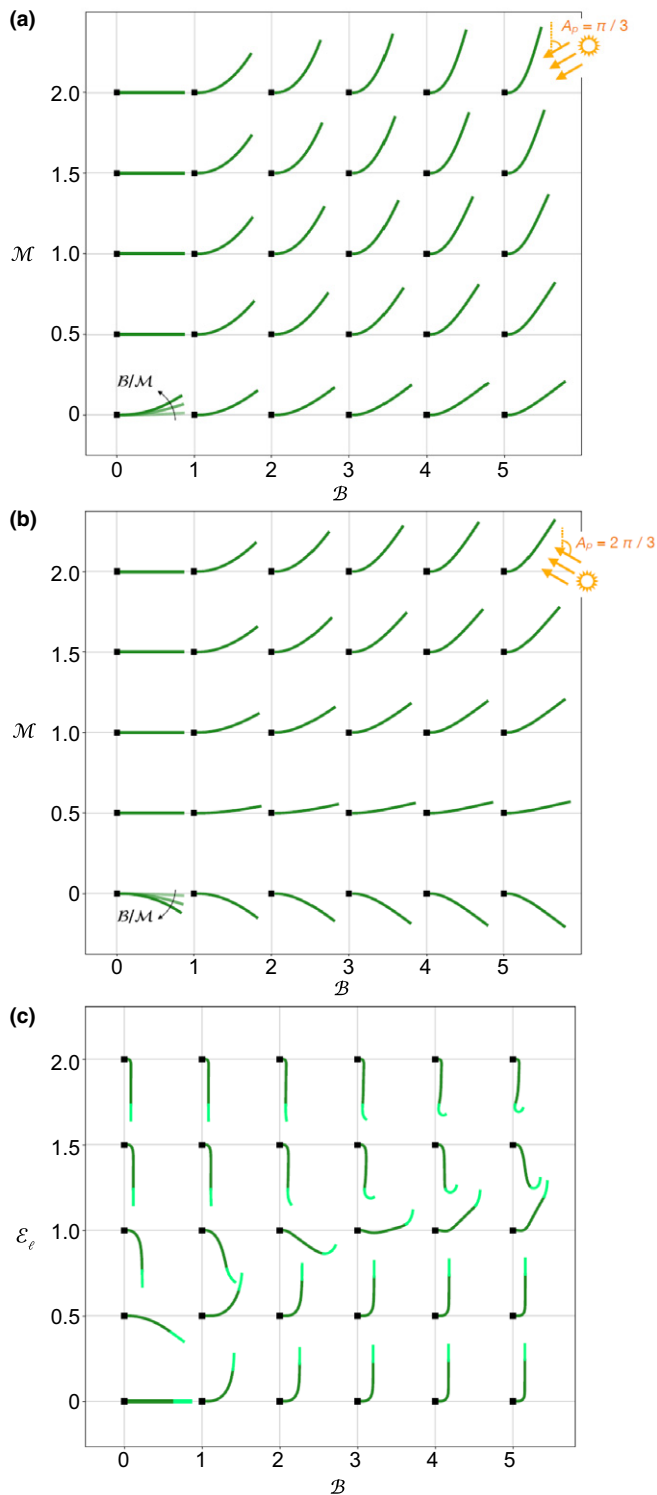


**Fig. 7** Morphospaces generated in the  $A_iC$  and  $AC\hat{E}-\hat{E}_i$  models by varying the balance number,  $B$  the motion pointing number  $\mathcal{M}$  and the elastic sagging number  $\mathcal{E}_i$ . (a, b)  $B - \mathcal{M}$  morphospaces in  $A_iC$  (Bastien *et al.*, 2015): steady-state shapes generated by varying the balance number  $B$  and the motion pointing number  $\mathcal{M}$  in the  $A_iC$  (photo-graviproceptive) model. The light source is either from above  $A_p = \pi/3$  (a) or from below  $A_p = 2\pi/3$  (b). Changing  $A_p$  demonstrates the phenotypic plasticity of the shape and posture (note that  $\mathcal{M}$  is also function of the intensity of the blue light impinging the organ, providing another source of plasticity). The influence of  $B$  and  $\mathcal{M}$  demonstrate the genetic control over shape and posture. (c)  $B - \mathcal{E}_i$  morphospace generated by the  $AC\hat{E}-\hat{E}_i$  model (graviproceptive drive and elastic sagging). This morphospace is slightly different from the morphospace found in (Chelakkot & Mahadevan, 2017), because of two additional hypotheses: (1) we considered a realistic range of proprioceptive sensitivity to avoid curvature fixation, as found by Bastien *et al.* (2015); and (2) mechanical buckling was avoided with important rigidification after maturation (in plants, this is controlled by lignification and eventually secondary growth). Note that for all the shapes in (a–c), the gravitropic set-point angle ( $A_{GSA}$ ) is zero and the weeping number  $\mathcal{W}$  is zero too (no antigravitropic curving). Altogether, the range of possible shapes generated by varying,  $B$   $\mathcal{M}$  and  $\mathcal{E}_i$  is huge, varying from orthotropic to plagiotropic and even apparently negatively tropic (sagging) shapes.

these traits at the organ cross-section level, it is then possible to zoom and focus in on the crucial cellular and molecular processes that are involved in the control of these four key parameters of global dynamics (Tardieu, 2003). Indeed, they have three important properties: they are dimensionless, integrative and intensive.

Dimensionless quantities such as  $\mathcal{B}\mathcal{M}\mathcal{W}\mathcal{E}_i$  are very useful in natural sciences, whether in physics, chemistry or biology (see Ortega, 2018 for an example in plant science). Indeed, they ‘unease’ the understanding of the interplay between phenotypic variables in setting a process. They also make it possible to compare different systems that might not otherwise seem directly comparable (e.g. plants of different species, size, stage, age, etc.) (Hollender *et al.*, 2018b).

$\mathcal{B}\mathcal{M}\mathcal{W}\mathcal{E}_i$  are clearly integrative traits: they include all the relevant information for shape control. As intensive parameters, they do not depend on the size of the plant: plants with the same  $\mathcal{B}\mathcal{M}\mathcal{W}\mathcal{E}_i$  in the same conditions display similar shapes.

Finally, they are not affected by the amount of the environmental stimulus (such as tilt).  $\mathcal{M}$  depends on the characteristics of the light: intensity of BL and red:far red (R:FR) ratio; but the parameters of the  $\mathcal{M}(l)$  function do not. Therefore the  $\mathcal{B}\mathcal{M}_{(l)}\mathcal{W}\mathcal{E}_i$  quadruplet is therefore an excellent macroscopic set of phenotypic traits (Tardieu, 2003) with which we can study quantitatively the genetics of shape control. All of them can be readily phenotyped quantitatively (Bastien *et al.*, 2013, 2016; Coutand *et al.*, 2019; Moulia *et al.*, 2019).  $\mathcal{B}$  and  $\mathcal{E}_i$  can even undergo high-throughput phenotyping (Bastien *et al.*, 2013; de Langre *et al.*, 2019).

The  $\mathcal{B}\mathcal{M}_{(l)}\mathcal{W}\mathcal{E}_i$  quadruplet controls clearly adaptive processes (the balance and the light foraging of the plant) and some hints for their natural selections have been found (Bastien *et al.*, 2014). They could be used to investigate the effects of major genes (e.g. *TAC1*, *LAZY* and *WEEP*; Hill & Hollender, 2019). It is indeed tempting to relate the *TAC1/LAZY* balance to the control of the balance number  $\mathcal{B}$  (*LAZY*?) and the motion pointing number  $\mathcal{M}$  (*TAC1*?). *WEEP* could be modulating the weeping number,  $\mathcal{W}$  acting either

possibly four traits the  $\mathcal{B}\mathcal{M}\mathcal{W}\mathcal{E}_i$  quadruplet if lateral axes with an antigravitropic curving rate are included.

These four shape-driving numbers are traits that are defined at the scale of a ‘slice of organ’ (one-cell-thin stem segment or cross-section; Peyhardi *et al.*, 2017), that is the *minimal module of shape regulation, a kind of multicellular apparatus*. This module includes several tissues (e.g. for  $\mathcal{B}$ : the statocytes, proprioocytes, the lateral auxin transport and the actuating tissue; Moulia *et al.*, 2019). From

on the antigravitropic curving rate  $\kappa_{\text{AGO}}$ , or on the proprioceptive sensitivity  $\gamma$ . However, this  $\mathcal{BM} - \mathcal{W}$  hypothesis remains to be tested.

Additionally, the question of how these internal and environmental effects may be involved in the dynamic control of branch shaping in the different architectural models of branch patterning (Fisher & Stevenson, 1981) remains to be elucidated. Moreover, the link between tropisms in lateral branches and the resulting crown shape is puzzling. However, some insights have been gathered recently on the link between axis shaping and the dynamics of crown shaping.

## V. What controls the shaping of the crown edge?

### 1. Mechanistic ingredients of crown morphogenesis

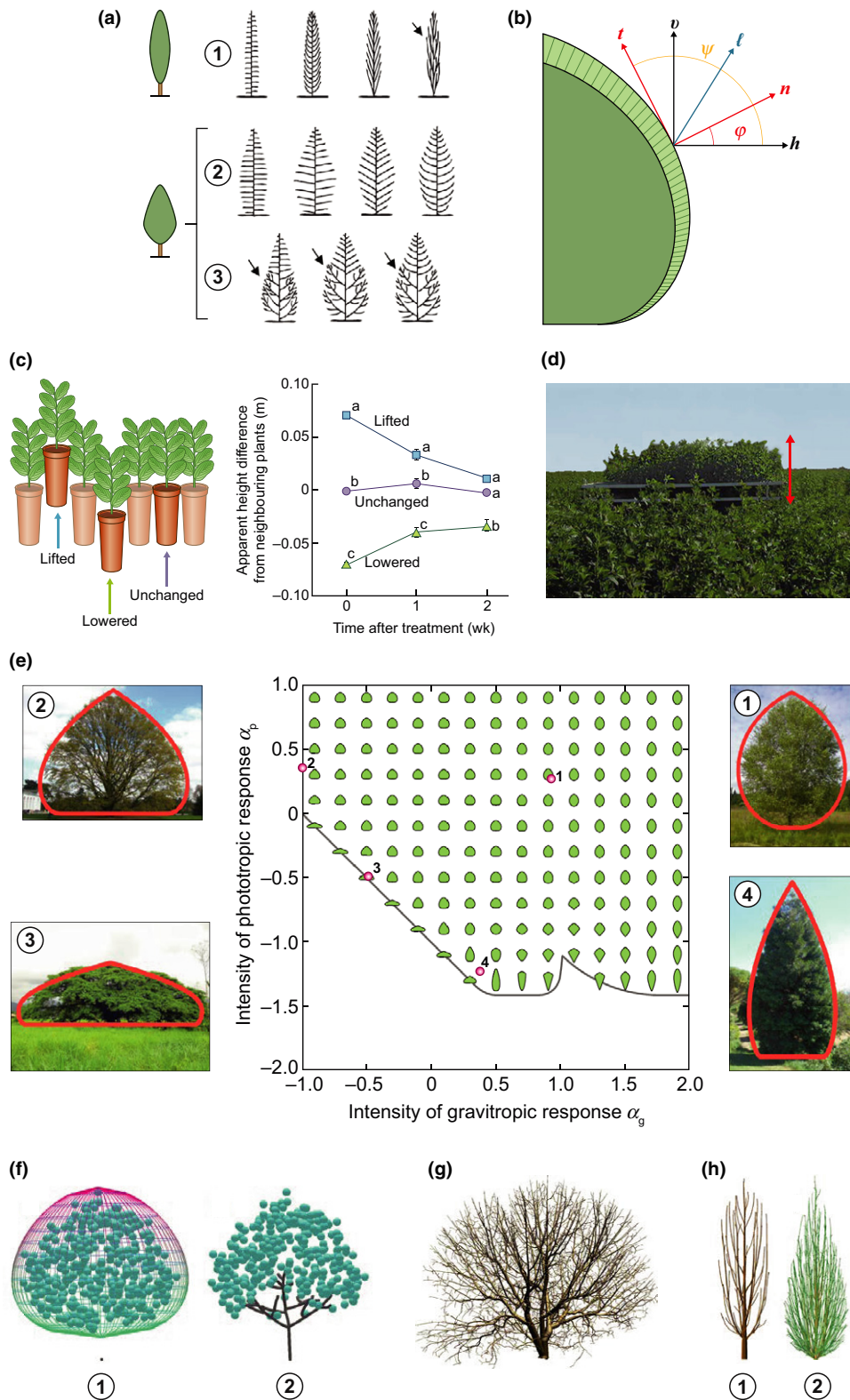
**Branching display or front expansion? The duality of crown development** From the fact that a crown builds up out of the branching process, it may seem obvious *a priori* that the shape of the outer contour of the crown results from the iterative branching, so that the control of crown shape is to be sought into that of branching. Because of the branched architecture, the geometrical parameters of the central axes (e.g. angle and length of the trunk and of the scaffold branches) would have more influence on crown shape compared with that of peripheral one, the small outer twig. This is consistent with what arboriculturists call ‘formative pruning’, which targets the young scaffold branches in the young tree to shape the adult tree crowns (Kerr & Morgan, 2006). However, this *a priori* displays various caveats.

Indeed, Barthelemy & Caraglio (2007) nicely pointed out that similar steady crown shapes can be reached through very different branching patterns (Fig. 8a). It is also striking that the symmetry of the outer shape of the crown is often higher compared with that of the bearing branching system (Leonardi & Stagi, 2019). In addition, a study of how the LIGNUM model based on branching processes and ecophysiological functions could fit real crowns, Sievanen *et al.* (2018) concluded that it was necessary to modify the local number of lateral buds as a function of local density in the crown to yield a correct simulation of its shaping; a conclusion also reached by Eloy *et al.* (2017). A centralised and fixed branching pattern could not yield a proper shaping. Finally, from what we have seen before for axis morphogenesis, a large part of the crown shaping may occur at places where primary growth, tropism and strong light heterogeneities occur. Moreover, only growth at the edge of the crown outline can change its shape (inner events only affect the crown density). Altogether, this points at a possible key mechanism of crown shaping at the peripheral growth front of the crown, involving the tropic direction resulting from the PGSA of the branch growth zones sitting near the crown outline (Fig. 9b; Duchemin *et al.*, 2018).

**An outline smoothing mechanism : shoot elongation convergence** Having defined the relevant growth front of the crown, another question is: ‘What can prevent this growth from breaking the outline into independent parts, that is destabilising the continuous and regular front?’

This is achieved through a coupling between the growth of neighbouring branches that reduces their ‘size inequality’, a process known as ‘shoot elongation (spatial) convergence’. Through very elegant experiments using canopies of potted plants that could be lifted up or brought down (Fig. 8c); Nagashima & Hikosaka (2011) demonstrated that the shoot elongation of the neighbouring plants converged, so that the height differences across the canopy decreased over time and the top of the canopy was finally flat again. This was found in a wide range of species (tobacco and *Arabidopsis* seedlings, cucumber seedlings, *Chenopodium*, *potentilla*). It involved a control of the elongation growth depending on two signals : (1) a photomorphogenic response to the sensing of neighbours through their reflected red : far red ratio, and acting through phytochrome PhyB, resulted in a convergence of height growth (Ballare *et al.*, 1994; Ballare & Scopel, 1997; Shibuya *et al.*, 2013); and (2) a wind-sensing thigmomorphogenic signal (as outliers experience a higher bending under wind drag and are able to sense it) (Nagashima & Hikosaka, 2012). Indeed, Moulia & Combes (2004) showed in an alfalfa field that reducing the wind-induced bending in a patch of canopy (Fig. 8d) allowed a dramatic outgrowth of the patch. However, the patch remained mostly flat due to a similar within-patch wind stimulation and to red/far red photomorphogenic coupling. This double control explains how the canopy top of monogenotypic crops can be so flat. To our knowledge, this has never been assessed in tree species. But it seems reasonable to assume that this is also the case, as shade avoidance and thigmomorphogenic mechanisms have been described in some tree species such as poplar (Karve *et al.*, 2012; Moulia *et al.*, 2015). Indeed monogenetic tree-sapling canopies showed a strong homogeneity in height between neighbours and finally a flat canopy. In addition, it was found that shoot elongation was more coupled when shoots displayed a similar morphology and were therefore likely to be genetic relatives (Crepy & Casal, 2015; Till-Bottraud & de Villemeureuil, 2016), so this effect is likely to be enhanced for the genetically similar twigs within a crown.

An analogy can be drawn with the role of surface tension in the physics of a famous morphogenetic process: the viscous fingering process, which is the formation of patterns at the interface between two fluids in a porous medium (known as Saffman–Taylor dynamics; Duchemin *et al.*, 2018). Indeed shoot length spatial convergence, stabilising the front dynamics and smoothing out the front shape by damping the velocity fluctuations, has a similar role to surface tension in Saffman–Taylor dynamics (see for example Raj (2016) [https://www.youtube.com/watch?v=9Flsy0sc\\_cg](https://www.youtube.com/watch?v=9Flsy0sc_cg)). However, this analogy is only partial as shoot elongation convergence results from biological signalling processes, whereas Saffman–Taylor dynamics results from a purely physical interaction between solid–liquid/liquid–liquid involving energetic–entropic processes (such as surface tension). In addition, it smooths out divergences in growth velocities and not in the static shapes. However, this analogy has driven crown research a step further ahead into the possibility of considering crown shaping as resulting from a continuous growth front, in which inner growth will provide the ‘push’, while the ‘shoot elongation convergence’ will keep the growth front as smooth as possible.



## 2. The crown front model

Stepping on the considerations above, Beyer *et al.* (2014) proposed to consider the crown as a continuous medium. Moreover, Duchemin *et al.* (2018) proposed to adapt the  $A_rC$

model considering that the front dynamics runs perpendicular to the elongation zone of each branch reaching the actual crown outline. In this crown front model (CF<sub>m</sub>), the growth velocity of the crown edge  $U$  at each point on the front (Fig. 8b) becomes:

**Fig. 8** Crowns: process-based dynamical modelling. (a) Similar crown shapes with different branching patterns observed in the different architectural types of *Cupressus sempervirens*: ① fastigiate, ② and ③ intermediate crown shape groups (black arrows indicate reiterated complexes). (b) Geometrical specification of the crown front model  $CF_m$ :  $\mathbf{v}$ : vertical,  $\mathbf{h}$  horizontal,  $\mathbf{n}$ : normal to the crown,  $\mathbf{t}$  tangent to the crown,  $\mathbf{l}$  main direction of light,  $\Psi$  aperture angle ( $\mathbf{t}$ ,  $\mathbf{h}$ ), light green area shows the growth increment, and the green segments display the directions of growth. (c) Experimental demonstration of the shoot elongation convergence: with a stand of potted plants at the same stage and from the same genotype, a few test plants are lifted up, and others are lowered and the height difference to the unchanged neighbours is recorded (side graph) showing shoot elongation convergence. (d) Demonstration of the effect of wind-induced thigmomorphogenesis (mechanosensitive control of growth) in the shoot elongation convergence: with an alfalfa field (*Medicago sativa* L.): a square of plants were grown through a double mesh that reduced the amplitude of their wind-induced sway. As soon as the foliage of the plants was over the top mesh, its position was lifted up so that the distance between the mesh and the tip of the main shoot remained constant, resulting into a constant and reduced amplitude of wind sways. (e) Morphospace of crown shapes generated by the crown front model  $CF_m$ ;  $\alpha_g$  and  $\alpha_p$  are the intensities of the gravitropic and phototropic responses. Green shapes are converged steady-state and self-similar shapes. The pictures at the corners illustrate the comparison between real tree crowns and self-similar shapes from the  $CF_m$  model: ① *Betula pubescens*; ② *Quercus castaneifolia*; ③ *Enterolobium cyclocarpum*; ④ *Thuja occidentalis*. The red curve represents the best  $CF_m$  fit. (f) Space colonisation algorithm driving an L-system model of architectural development (SCa-L-Tree): ① Envelope with the attraction points along the crown front and the initial tree node. ② Generation of the tree skeleton: branches occurs where attraction points are available and occupy them so that they become inaccessible to the other branches. (g) A tree generated by SCa-L-Tree using continuously added attraction points, and general cylinder following the pipe model. (h) Influence of the shape of the crown on the resulting branch pattern: ① columnar shape, ② conically oval shape, compared also with the broadly rounded shape (g). (a) From Barthelemy & Caraglio (2007). (b, e) From Duchemin *et al.* (2018). (c) From Nagashima & Hikosaka (2011). (d) From the experiment described in Moulia & Combes (2004). (f–h) From Runions *et al.* (2007).

$$U = \psi \frac{\mathbf{n} + \alpha_g \mathbf{v} + \alpha_p \mathbf{l}}{|\mathbf{n} + \alpha_g \mathbf{v} + \alpha_p \mathbf{l}|} + \gamma_{lc} \kappa_o \mathbf{n} \quad \text{Eqn 18}$$

where  $\mathbf{n}$  represents the outward normal unit vector,  $\mathbf{l}$  is the unit vector indicating the direction of light,  $\mathbf{v}$  is the upward vertical unit vector. Bold characters mean a vector.  $\alpha_g$  and  $\alpha_p$  are the intensity of the gravitropic and phototropic responses respectively,  $\psi$  is the amount of light reaching this point (estimated as equal to the aperture angle; Fig. 8b), taking into account the self-shading of the crown.

The first part of the right term of Eqn 18 states that the growth rate is proportional to the amount of light  $\psi$ , and deviates from the normal direction of the crown depending on a photogravitropic term  $\alpha_g \mathbf{v} + \alpha_p \mathbf{l}$ . Note that  $\alpha_g$  and  $\alpha_p$  are related to the gravitropic sensitivity  $\beta$  and the phototropic sensitivity  $\nu$  of the  $A_rC$  model. More precisely  $\alpha_g \mathbf{v} + \alpha_p \mathbf{l}$  is related to the PGSA as defined in Eqn 5 and therefore to the motion pointing number  $\mathcal{M}$ . Note that the effects of active weeping and passive elastic sagging, as well as the straightening effect of proprioception, are neglected.

The second part of the right term of Eqn 18 is the smoothing term related to shoot elongation convergence. It states that if the local surface curvature  $\kappa_o$  on the crown is negative (the crown makes locally a small convex bulge), then the velocity  $\mathbf{U}$  in the normal direction  $\mathbf{n}$  becomes reduced. By contrast, if the surface curvature  $\kappa_o$  is positive (the crown makes locally a small concave sinkhole), then the normal growth speeds up. Altogether, this restricts the onset of ‘fingers’ in the crown and keeps it smooth.  $\gamma_{lc}$  is not related to the proprioceptive sensitivity  $\gamma$  of the subtending axis. We kept the same symbol for consistency with the original publication, but also because this is another example of an active control of the curvature, involving here red/far red sensing and photomorphogenesis.

The amount of light  $\psi$  and the average direction of light  $\mathbf{l}$  can be calculated easily from simple geometrical optics as the angle of view of the sky that is not obscured by the neighbouring parts of the crown (see Fig. 8b) or by the ground (both being assumed to completely absorb the light, a very good approximation for the BL waveband involved in phototropism; Combes *et al.*, 2007). This provides feedback from the global shape of the crown onto the local growth

rate. As shown in Fig. 8(b), when considering a point at the bottom of the crown, the crown above obscures a large part of the sky and the crown front at this point will grow slowly. By contrast, if we now consider a point on the top of the crown, it will see the whole sky, and grow fast in the vertical direction (as  $\mathbf{l}$  is collinear to  $\mathbf{v}$ ).

The major finding of this study is that the  $CF_m$  converges in many cases to a steady-state shape that does not depend on the initial shape but only on the intensity of the gravitropic and phototropic responses  $\alpha_g$  and  $\alpha_p$ . In other words, the successive crowns are self-similar, only changing by a scaling coefficient over time, therefore keeping the same shape.

Fig. 8(e) is the morphospace for crowns generated by the  $(\alpha_g, \alpha_p)$  phenotypic set. Green shapes correspond to computations that have converged towards self-similar steady state. A closed-form analytical solution of the  $CF_m$  could be found using a similar approach to that used for crystal growth in physics (Wulff construction; Duchemin *et al.*, 2018). Green shapes display a large diversity of shapes as a function of the parameter sets  $(\alpha_g, \alpha_p)$ , showing that the (genetic) variations in the sensitivities to phototropism and gravitropism in the  $CF_m$  can indeed produce different theoretical crown shapes.

### 3. And its assessment

The  $CF_m$  computations were assessed vs the real tree crowns observed in nature for 36 species, sampling the genetic diversity of angiosperm broadleaf trees from different biomes (tropical and temperate trees). Care was taken to consider only fully isolated trees with: (1) no traumatism (e.g. artificial or accidental pruning due to wind, herbivory of man action and leading to traumatic reiteration); and (2) at a development stage close to the architectural unit (a stage at which all the types of axes that the species can develop have been differentiated; Barthelemy & Caraglio, 2007) or to the fully mature crown. Fig. 8(e) shows that for 75% of the cases, the fit is fair with parametric values of  $(\alpha_g, \alpha_p)$  both positive (as expected from the physiology of phototropism and gravitropism). This is not a complete and independent validation of the  $CF_m$  model. A full validation would require detailed kinematical records of crown growth in isolated trees, as now allowed by the novel 3D digitisation

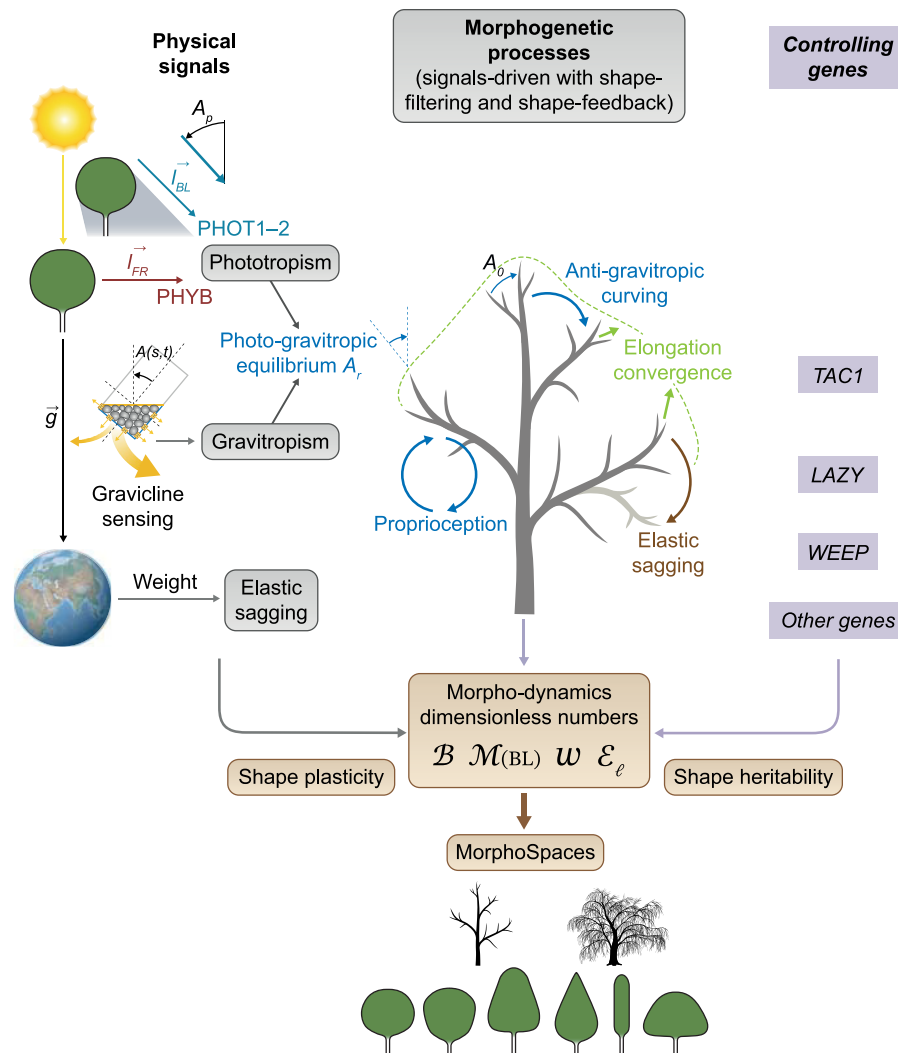


**Fig. 9** Summary figure. The shaping of plant axes and crowns through tropisms and elasticity. Two external physical signals, gravity and light, drive the gravitropic and phototropic morphogenetic processes, leading to a photogravitropic equilibrium shape of each axis. Light can be modified by the shade of the crown itself, leading to a top-down feedback from the global shape of the crown to the local shaping of the plant axes. Further feedbacks from the axis shape (proprioception), and from the interactions between neighbouring shoots within the crown (elongation convergence) modify these reactions and drive a convergence to smooth axis and crown shapes. At the same time, the influence of the topological relation of each shoot with its parent shoot through active anti-gravitropic curving drives a continuous angular divergence of lateral shoots from the direction of their parents. Finally, the resulting shape may be modified by passive elastic bending. Thanks to modelling, the interplay of these morphogenetic processes can be reduced to a quadruplet of dimensionless numbers,  $B, M_{(BL)}, W, E_l$ , which together control the steady-state shape and posture of each axis, and finally the shape of the whole crown. Being independent of plant size and of the plant environment, they are traits of choice for unravelling the function of genes such as *TAC1*, *LAZY* or *WEEP*. Once the angle of insertion at the basis of each axis  $A_0$  (initial condition), the angle between the gravity direction and the light direction  $A_p$ , and the light intensity and quality (physical signals acting as environmental drivers) are given, the  $B, M_{(BL)}, W, E_l$  quadruplet describes the morphospace of possible shapes and their achievement through growth. Therefore, these four traits are likely to be the target of natural and artificial selection. Finally, the balance between shape plasticity and heritability is explained by the fact that: (i) heritable  $B, M_{(BL)}, W, E_l$  control the plastic response to light and gravity; and (ii) top-down feedbacks for the global shape channel the morphogenesis of axes and crowns. blue, dark red and black thin arrows: vectorial environmental cues sensed by the plant ( $g$ , gravity;  $I$ , monochromatic or polychromatic light beams); turquoise blue and green arrows: biological processes allowing for shape filtering and shape feedback, brown arrows: physical/mechanical passive processes; yellow arrow, sunlight beam; golden-yellow arrows, auxin fluxes.

and shape fitting techniques. Nevertheless, it shows that the photogravitropic hypothesis of crown shaping through photogravitropic growth at the periphery of the crown is probably holding as a relevant model.

In addition, negative values of  $\alpha_p$  (i.e. negative phototropism) were required to fit the remaining 25% of the cases studied by Duchemin *et al.* (2018). Negative phototropism in light-grown

shoots is not documented in the literature except in some artificial mutants with reduced auxin levels (Sato *et al.*, 2014). Therefore, apparent negative values of  $\alpha_p$  may reflect cases in which the active weeping or passive sagging down of the lateral branches should not be neglected (although no obvious weeping genotype has been included in the assessment set, some weeping or sagging of lateral branches is likely to be present).

The computations of the  $CF_m$  model bring new puzzling questions. Indeed, it was assumed that the sky-light was homogeneous (such as the one provided by an overcast sky on cloudy days; Li, 2010). This is not a necessity for the  $CF_m$ , but it made the calculations straightforward. However, in regions where sunny days have a significant share of the lighting, this is not realistic. Including a direct sunlight component in the  $CF_m$  model would clearly break the axisymmetry of the crown shape due to a faster growth in the sun-facing side. However, this is not observed in most isolated trees, whatever the region of the world! Duchemin *et al.* (2018) argued that sensing of the red : far red ratio through phytochrome PhyB compensated for light intensity, and that this sensing may be what is behind the photomorphogenetic control of the crown front velocity by light. However, this would mean that the  $CF_m$  model should take into account far red light (which is reflected highly by the neighbouring leaves) in the calculation of (1) the amount of light  $\psi$ ; and of (2) the average direction of light  $l$ . This hypothesis remains to be tested. From a broader point of view, this issue of the resilience of crown axisymmetry is an interesting question that has never been investigated. Why are most of the tree crowns in nature not biased towards the sun (with the exception of *Araucaria columnaris*; Johns *et al.*, 2017) despite the huge influence of light on growth and form?

#### 4. Major insights

Although open questions remain, the  $CF_m$  model provides several insights. The first is, of course, that crown shaping can be controlled through tropisms, and only tropisms. The emergence of the typical shapes comes through the optical interaction of phototropic sensing with the actual shape (and its self-shading). One can see that this is an autocorrective process: thanks to shoot elongation convergence, this control can even allow the plants to recover from hazardous shedding of a part of the crown (through wind or artificial pruning, herbivory attack, etc.). It also explains the frequent observation that a grove of two to three trees can build a canopy in which the outer shape is very similar to the outer shape of the crown of a single tree. Finally, it suggests a possible genetic control. If we assume that the  $CF_m$  model of photogravitropic crown shaping captures an important control, then we may revisit the action of *TAC1* and *LAZY* genes at the crown level (Busov, 2018; Hill & Hollender, 2019). Indeed, as shown in Fig. 3(a–f), mutations in these genes do not only affect the gravitropic component of the lateral branches; but they also result in major changes in tree crown shape.

#### 5. From crown shape to branch shape?

Finally, these crown studies reset the question of the duality between crown shaping and branching. Interestingly, Duchemin *et al.* (2018) computed the distribution of branch growth direction that would correspond to the successive growth velocity vectors  $\mathbf{U}$  (Fig. 8b). They concluded that a change in gravisensitivity leads to steeper branch angles, as observed in the *tac1* mutants, shown in Fig. 3(d,f).

Going a step further, Runions *et al.* (2007) investigated the possibility to infer realistic branching patterns from the outer shape of the crown in 3D using a space colonisation algorithm driving a L-system model of architectural development (SCa-L-Tree). They assumed that the crown envelopes define sites of free space that the branch growth tends to fill (Fig. 8f). The crown is then discretised into attracting free spaces. Then, the tree is generated through an algorithm of branching implemented into an L-system, in which branching rate and branch elongation are favoured near free spaces. In this way, whenever a branch reaches a free space, this space becomes occupied and does not subsequently attract other branches. This reverse control of the crown shape on branching yields amazingly realistic patterns of branching architecture (Fig. 8g), and setting different crown shapes leads to different and realistic sets of branching patterns (Fig. 8g,h). This shows that branching can be controlled by the actual crown shape and viewed as a crown-filling-(oriented) process.

However, there is much more than photogravitropic control at the crown surface for the control of the branched architecture of trees. The requirements for light interception, wind firmness and water conduction, and the way they influence the morphogenesis of the branch scaffold making the crown, all need to be investigated. Some models have been developed to do this analysis (Tardieu, 2003; Vos *et al.*, 2010; Prusinkiewicz & Runions, 2012). More recently an Eco-Evo-Devo approach of the emergence of fitted and plastic tree architectures through selection by wind and light competition using virtual simulation has been proposed (Eloy *et al.*, 2017). However, detailing all this approach would require a complete specific review. In addition, we can just indicate that they point out the major role of physical signals, such as light or mechanical stimulations, in the architectural development, through photomorphogenesis and thigmomorphogenesis. These signals are mediated through their distribution in plant architecture and, for both light and wind, the size of the crown and the shape of its edge are crucial.

## VI. Conclusion

From this review of the shaping of axes and crown, a few major features have emerged, that can probably be generalised to include all post-SAM morphogenesis.

The first feature is methodological. Clearly, the recent interdisciplinary crosstalk between physics, ecophysiology, genetics, functional genomics and functional modelling is beneficial. Just as for the SAM morphogenesis, it has started lifting important locks that none of the disciplines alone would have achieved. In this process, modelling has proved to be a key tool for disentangling the different controls and then studying their interactions and integration. Dimensional analysis, also borrowed from physics, has shown its power too. This was illustrated by the demonstration that the shaping of axes depends mostly on three dimensionless numbers,  $\mathcal{B}\mathcal{M}\mathcal{E}_l$  (balance number, motion pointing number and elastic sagging number), adding  $\mathcal{W}$  (the weep number) for lateral axes (Fig. 9).

A major insight gathered through this methodology is the effect of global shape as an input to the local morphogenetic process (just as found for the SAM; Hamant & Mouliat, 2016). A first level of

such global shape effect is an amplifying effect. Indeed local changes generate global effects on shapes and affect the inputs of local regulation elsewhere. This is clearly illustrated at the level of the axis: gravitropic bending at a basal place prevents the more apical pieces of the stem achieving their GSA through a lever-arm effect on motion, ruining the possibility of pure gravitropic control (Bastien *et al.*, 2013; Dumais, 2013; Okamoto *et al.*, 2015). Another such amplifying effect is mechanical bending and the risk of breaks in scaffold branches and trunks that experience a lever-arm effect, amplifying mechanical stresses (Mouliia *et al.*, 2015; Chelakkot & Mahadevan, 2017).

However, this has been counteracted by a set of negative feedback mechanisms that allow for shape convergence, similar to that observed in the SAM (Hamant & Mouliia, 2016). At the scale of a single axis, this involves mechanosensitive proprioception that drives the straightening of axes. At the scale of the crown, this involves spatial shoot elongation spatial convergence, implying both photosensing of the neighbouring axes and mechanosensing of the escape from wind shielding from neighbouring axes. Finally, thigmomorphogenetic control of secondary growth enables coping with the lever-arm effect at the level of each axis, but also at the plant architecture level (Mouliia *et al.*, 2015; Eloy *et al.*, 2017). The two first mechanisms (proprioception and photomorphogenetic spatial shoot elongation convergence) only involve shape sensing (mechanical or optical), whereas the two others (thigmomorphogenetic shoot elongation convergence and thigmomorphogenetic control over secondary growth) involve the interaction of wind with the actual shape. In this way, these shape feedback mechanisms bring back an effect of the upper scale to the lower one. The shape of an axis cannot be fully understood without taking into account the dynamics of the crown and the signalling that is continuously modified by this dynamics. Moreover, amplifying and feedback effects altogether provide nonlinearity to the morphogenetic responses, allowing for a larger shape repertoire. These result in spatial heterogeneities, even with identical local mechanisms. It is shape sensitivity that provides heterogeneous distribution of curvature along a lateral plant axis. By the same token, it is crown shape feedback through optical and mechanical signals that produces a nonhomogeneous distribution of branch orientations with steeper branches at the top and more plagiotropic branches at the bottom (Fig. 9).

This clearly points out another major feature of the post-SAM morphogenesis of axes and crown shapes: the crucial part of physical signals acting through sensing, in particular light sensing, gravity sensing and the sensing of curvature (Fig. 5a). Although not reviewed here, temperature should be added to the list as evidence of thermomorphogenesis and its interactions with photomorphogenesis and tropisms are becoming quite clear (Roychoudhry *et al.*, 2017; Casal & Balasubramanian, 2019). In addition, taking fully into account the effect of wind on axis and crown shapes (including the extreme cases of anemomorphosis; Fig. 3j) remains to be achieved (Telewski, 2012; Eloy *et al.*, 2017). Altogether, the dependence of morphogenetic processes on these physical signals is the key to phenotypic plasticity, while their control through dimensionless numbers, and ultimately genes, accounts for the shape heritability, especially in isolated plants (Fig. 9).

It should be noted also that the two physical signals we have studied here are complex signals bearing several cues. Light brings a set of signals that act through photomorphogenesis and phototropism. Mechanical signals also bring a complex of signal acting through gravicline sensing, proprioceptive sensing, but also through thigmomorphogenesis and eventually thigmotropism (i.e. tropic response to anisotropic mechanical stimulations, as for example by wind drag; Telewski, 2012; see Fig. 3j). However, in any case, their actions are mediated by the actual shape of the plant. Light is filtered through the shading/reflective effect of the shape. Mechanical signals are transferred/filtered or amplified through the biomechanical structure of the plant. This mediation is necessary for shape control.

Two major emergent behaviours have also being highlighted: the control of shape smoothness (and the lowering of crown curvature) and the symmetry-keeping mechanisms. Most morphogenesis in the SAM and leaves is about pattern formation (i.e. symmetry breakages and bifurcations). Here, however, morphogenesis is also about avoiding bifurcations and symmetry breakage: how do orthotropic axes not buckle under their own weight in most cases? How do crowns not undergo Saffman–Taylor-like instability (with shoot elongation spatial convergence restraining the outgrowth more efficiently than surface tension)? How do crowns and trunks keep their symmetries despite the asymmetry of light and temperature, but give way to the asymmetry of directional wind? These major questions need to be tackled. Moreover, in addition to these conservative shape-keeping mechanisms, plant shoot morphogenesis also displays a very high amount of shape plasticity (Fig. 3h–j), and these mechanisms are under active investigations.

Finally, as these interdisciplinary studies of post-SAM morphogenesis are fairly recent, there are still many things that need further investigation.

We still do not understand the processes and mechanisms involved in the orthotropic/plagiotropic differentiation of the axis (Barthelemy & Caraglio, 2007). The link between (1) *BM.WE<sub>1</sub>*, and (2) *TAC1*, *LAZY* and *WEEP* genes, and more generally the controlling gene networks, remains to be investigated. A method of zooming from the macrocharacters (such as *BM.WE<sub>1</sub>*) to the controlling genes is therefore necessary. However, we now have a framework for that (Figs 5, 8, 9) that relies on modelling. Indeed, modelling allows a top-down focus on the controlling tissues/cells and on the regulatory mechanisms (Tardieu, 2003; Mouliia *et al.*, 2015), which in this case should involve auxin transport and the proprioceptive pathway. In addition, this zooming from the macrocharacters to the controlling genes is also helped by model-assisted phenotyping (Bastien *et al.*, 2013; Coutand *et al.*, 2019) that enables a better inspection of the effects of gene variations (mutants or transgenics) and/or of the effects of environmental factors.

The links with the evolution of shapes and the possibility to go beyond the hypotheses of an optimal shape/size relationship to really investigate Evo-Devo aspects is also a promising avenue.

Because the concepts and tools are now available, we are hopefully witnessing a novel period of phytology/botany

development: from morphology to morphogenetics even beyond SAM. . . . As Douady *et al.* (2009) stated:

‘The study of organic shapes should be considered, not only as the trace of a prehistoric state of botany, a compilation of the diversity of shapes, but as a study of key ingredient in the dynamics of living organisms.’

We hope that this review will help to build up this exciting momentum!

## Acknowledgements

This research was supported by the CNRS (Mission pour l'Interdisciplinarité, project ARBRE), the GDR Phy.P «Bio-physique et biomécanique des plantes» (no. 2007) and the French government IDEX-ISITE initiative 16-IDEX-0001 (CAP 20-25) through the ‘Stand-up!’ project of Challenge 1 Deliverable 4. BM also acknowledges the support received from ANR Blanc Grap2 (ANR-13-BSV5-0005-01), and the ‘fondation des Treilles’ where this project was designed. RB acknowledges the support from the Bettencourt Schueller Foundation, through his CRI Research Fellowship. The authors thank the editor Naomi Nakayama, the four anonymous reviewers and the Senior Commissioning Editor Holly Slatter for the very useful and constructive input into building this review, and to have allowed sufficient space for the physics or modelling aspects to be presented in a manner accessible to biologists, in a truly interdisciplinary spirit.

## ORCID

Eric Badel  <https://orcid.org/0000-0003-2282-7554>  
 Renaud Bastien  <https://orcid.org/0000-0002-5438-4287>  
 Laurent Duchemin  <https://orcid.org/0000-0001-8179-4452>  
 Christophe Eloy  <https://orcid.org/0000-0003-4114-7263>  
 Bruno Moulia  <https://orcid.org/0000-0002-3099-0207>

## References

- Almeras T, Fournier M. 2009. Biomechanical design and long-term stability of trees: morphological and wood traits involved in the balance between weight increase and the gravitropic reaction. *Journal of Theoretical Biology* 256: 370–381.
- Almeras T, Gril J, Costes E. 2002. Bending of apricot tree branches under the weight of axillary growth: test of a mechanical model with experimental data. *Trees-Structure and Function* 16: 5–15.
- Alonso-Serra J, Shi XP, Peaucelle A, Rastas P, Bourdon M, Immanen J, Takahashi J, Koivula H, Eswaran G, Muranen S *et al.* 2020. ELIMAKI locus is required for vertical proprioceptive response in birch trees. *Current Biology* 30: 589–599.
- Ballare CL, Pierik R. 2017. The shade-avoidance syndrome: multiple signals and ecological consequences. *Plant, Cell & Environment* 40: 2530–2543.
- Ballare CL, Scopel AL, Jordan ET, Vierstra RD. 1994. Signaling among neighboring plants and the development of size inequalities in plant populations. *Proceedings of the National Academy of Sciences, USA* 91: 10094–10098.
- Ballare CL, Scopel AL. 1997. Phytochrome signalling in plant canopies: testing its population-level implications with photoreceptor mutants of Arabidopsis. *Functional Ecology* 11: 441–450.
- Barbier FF, Dun EA, Kerr SC, Chabikwa TG, Beveridge CA. 2019. An update on the signals controlling shoot branching. *Trends in Plant Science* 24: 220–236.
- Barthelemy D, Caraglio Y. 2007. Plant architecture: a dynamic, multilevel and comprehensive approach to plant form, structure and ontogeny. *Annals of Botany* 99: 375–407.
- Bastien R, Bohr T, Moulia B, Douady S. 2013. Unifying model of shoot gravitropism reveals proprioception as a central feature of posture control in plants. *Proceedings of the National Academy of Sciences, USA* 110: 755–760.
- Bastien R, Douady S, Moulia B. 2014. A unifying modeling of plant shoot gravitropism with an explicit account of the effects of growth. *Frontiers in Plant Science* 5. doi: 10.3389/fpls.2014.00136.
- Bastien R, Douady S, Moulia B. 2015. A unified model of shoot tropism in plants: photo-gravi- and propio-ception. *PLoS Computational Biology* 11: e1004037.
- Bastien R, Legland D, Martin M, Fregosi L, Peaucelle A, Douady S, Moulia B, Hofte H. 2016. KymoRod: a method for automated kinematic analysis of rod-shaped plant organs. *The Plant Journal* 88: 468–475.
- Berut A, Chauvet H, Legue V, Moulia B, Pouliquen O, Forterre Y. 2018. Gravisensors in plant cells behave like an active granular liquid. *Proceedings of the National Academy of Sciences, USA* 115: 5123–5128.
- Beyer R, Letort V, Courneade P-H. 2014. Modeling tree crown dynamics equations with 3D partial differential equations. *Frontiers in Plant Science* 5: 329.
- Busov VB. 2018. Manipulation of growth and architectural characteristics in trees for increased woody biomass production. *Frontiers in Plant Science* 9. doi: 10.3389/fpls.2018.01505.
- Casal JJ, Balasubramanian S. 2019. Thermomorphogenesis. *Annual Review of Plant Biology* 70: 321–346.
- Chauvet H, Moulia B, Legue V, Forterre Y, Pouliquen O. 2019. Revealing the hierarchy of processes and time-scales that control the tropic response of shoots to gravi-stimulations. *Journal of Experimental Botany* 70: 1955–1967.
- Chauvet H, Pouliquen O, Forterre Y, Legue V, Moulia B. 2016. Inclination not force is sensed by plants during shoot gravitropism. *Scientific Reports* 6. doi: 10.1038/srep35431.
- Chehab EW, Eich E, Braam J. 2009. Thigmomorphogenesis: a complex plant response to mechano-stimulation. *Journal of Experimental Botany* 60: 43–56.
- Chelakkot R, Mahadevan L. 2017. On the growth and form of shoots. *Journal of the Royal Society Interface* 14. doi: 10.1098/rsif.2017.0001.
- Combes D, Bousquet L, Jacquemoud S, Sinoquet H, Varlet-Grancher C, Moya I. 2007. A new spectrogoniophotometer to measure leaf spectral and directional optical properties. *Remote Sensing of Environment* 109: 107–117.
- Costes E, Gion JM. 2015. Genetics and genomics of tree architecture. In: Plomion C, Adam-Blondon AF, eds. *Advances in Botanical Research, vol. 74. Land plants – trees*. the Netherlands: Science Direct 157–200.
- Coutand C, Adam B, Ploquin S, Moulia B. 2019. A method for the quantification of phototropic and gravitropic sensitivities of plants combining an original experimental device with model-assisted phenotyping: exploratory test of the method on three hardwood tree species. *PLoS ONE* 14: e0209973.
- Coutand C, Fournier M, Moulia B. 2007. The gravitropic response of poplar trunks: key roles of prestressed wood regulation and the relative kinetics of cambial growth versus wood maturation. *Plant Physiology* 144: 1166–1180.
- Creff A, Brocard L, Ingram G. 2015. A mechanically sensitive cell layer regulates the physical properties of the Arabidopsis seed coat. *Nature Communications* 6. doi: 10.1038/ncomms7382.
- Crepny MA, Casal JJ. 2015. Photoreceptor-mediated kin recognition in plants. *New Phytologist* 205: 329–338.
- d’Arcy Thompson W. 1917. *On growth and forms*. Cambridge UK: Cambridge University Press.
- de Langre E, Penalver O, Hémon P, Franchisse JM, Bogeat-Triboulot MB, Niez B, Badel E, Moulia B. 2019. Nondestructive and fast vibration phenotyping of plants. *Plant Phenomics* 2019: 1–10.
- Digby J, Firn RD. 1995. The gravitropic set-point angle (GSA): the identification of an important developmentally controlled variable governing plant architecture. *Plant, Cell & Environment* 18: 1434–1440.
- Douady S, Couder Y. 1996a. Phyllotaxis as a dynamical self organizing process. 1. The spiral modes resulting from time-periodic iterations. *Journal of Theoretical Biology* 178: 255–274.
- Douady S, Couder Y. 1996b. Phyllotaxis as a dynamical self organizing process. 2. The spontaneous formation of a periodicity and the coexistence of spiral and whorled patterns. *Journal of Theoretical Biology* 178: 275–294.
- Douady S, Manning A, Hennion B. 2009. In the beginning there was shape. In: Gérin M, Maurel MC, eds. *Origins of life: self-organization and/or biological evolution?* France, Paris: EDP Sciences, 47–60.

- Duchemin L, Eloy C, Badel E, Moulia B. 2018. Tree crowns grow into self-similar shapes controlled by gravity and light sensing. *Journal of the Royal Society Interface* 15. doi: 10.1098/rsif.2017.0976.
- Dumais J. 2013. Beyond the sine law of plant gravitropism. *Proceedings of the National Academy of Sciences, USA* 110: 391–392.
- Eloy C, Fournier M, Lacoite A, Moulia B. 2017. Wind loads and competition for light sculpt trees into self-similar structures. *Nature Communications* 8. doi: 10.1038/s41467-017-00995-6.
- van Es SW. 2020. Baby don't cry, genetic regulation of the weeping phenotype in *Prunus mume*. *Physiologia Plantarum* 170: 315–317.
- Fankhauser C, Christie JM. 2015. Plant phototropic growth. *Current Biology* 25: R384–R389.
- Fisher JB. 1985. Induction of reaction wood in *Terminalia* (Combretaceae) – role of gravity and stress. *Annals of Botany* 55: 237–248.
- Fisher JB, Stevenson JW. 1981. Occurrence of reaction wood in branches of dicotyledons and its role in tree architecture. *Botanical Gazette* 142: 82–95.
- Galland P. 2002. Tropisms of *Avena* coleoptiles: sine law for gravitropism, exponential law for photogravitropic equilibrium. *Planta* 215: 779–784.
- Gerttula S, Zinkgraf M, Muday GK, Lewis DR, Ibatullin FM, Brumer H, Hart F, Mansfield SD, Filkov V, Groover A. 2015. Transcriptional and hormonal regulation of gravitropism of woody stems in populus. *The Plant Cell* 27: 2800–2813.
- Godin C. 2000. Representing and encoding plant architecture: a review. *Annals of Forest Science* 57: 413–438.
- Goyal A, Karayekov E, Galvao VC, Ren H, Casal JJ, Fankhauser C. 2016. Shade promotes phototropism through phytochrome B-controlled auxin production. *Current Biology* 26: 3280–3287.
- Halle F, Oldeman RAA, Tomlinson PB. 1978. *Tropical trees and forests: an architectural analysis*. Berlin, Germany: Springer-Verlag.
- Hamant O, Moulia B. 2016. How do plants read their own shapes? *New Phytologist* 212: 333–337.
- Hamant O, Traas J. 2010. The mechanics behind plant development. *New Phytologist* 185: 369–385.
- Harrison CJ. 2017. Development and genetics in the evolution of land plant body plans. *Philosophical Transactions of the Royal Society B: Biological Sciences* 372. doi: 10.1098/rstb.2015.0490.
- Hartmann FP, Rathgeber CBK, Fournier M, Moulia B. 2017. Modelling wood formation and structure: power and limits of a morphogenetic gradient in controlling xylem cell proliferation and growth. *Annals of Forest Science* 74. doi: 10.1007/s13595-016-0613-y.
- Hill JL, Hollender CA. 2019. Branching out: new insights into the genetic regulation of shoot architecture in trees. *Current Opinion in Plant Biology* 47: 73–80.
- Hollender CA, Dardick C. 2015. Molecular basis of angiosperm tree architecture. *New Phytologist* 206: 541–556.
- Hollender CA, Hill JL, Waite J, Dardick C. 2020. Opposing influences of *TAC1* and *LAZY1* on lateral shoot orientation in Arabidopsis. *Scientific Reports* 10. doi: 10.1038/s41598-020-62962-4.
- Hollender CA, Pascal T, Tabb A, Hadiarto T, Srinivasan C, Wang WP, Liu ZC, Scorza R, Dardick C. 2018a. Loss of a highly conserved sterile alpha motif domain gene (*WEEP*) results in pendulous branch growth in peach trees. *Proceedings of the National Academy of Sciences, USA* 115: E4690–E4699.
- Hollender CA, Waite JM, Tabb A, Raines D, Chinnithambi S, Dardick C. 2018b. Alteration of *TAC1* expression in *Prunus* species leads to pleiotropic shoot phenotypes. *Horticulture Research* 5. doi: 10.1038/s41438-018-0034-15.
- Hung LF, Tsai CC, Chen SJ, Huang YS, Kuo-Huang LL. 2017. Strain distribution, growth eccentricity, and tension wood distribution in the plagiotropic and orthotropic branches of *Koeleruteria henryi* Dummer. *Trees-Structure and Function* 31: 149–164.
- Johns JW, Yost JM, Nicolle D, Igc B, Ritter MK. 2017. Worldwide hemisphere-dependent lean in Cook pines. *Ecology* 98: 2482–2484.
- Karve AA, Jawdy SS, Gunter LE, Allen SM, Yang XH, Tuskan GA, Wulschlegler SD, Weston DJ. 2012. Initial characterization of shade avoidance response suggests functional diversity between *Populus* phytochrome B genes. *New Phytologist* 196: 726–737.
- Kawamoto N, Kanbe Y, Nakamura M, Mori A, Morita MT. 2020. Gravity-sensing tissues for Gravitropism are required for 'anti-gravitropic' phenotypes of *Lzy* multiple mutants in Arabidopsis. *Plants* 9. doi: 10.3390/plants9050615.
- Kerr G, Morgan G. 2006. Does formative pruning improve the form of broadleaved trees? *Canadian Journal of Forest Research* 36: 132–141.
- Ko JH, Han KH, Park S, Yang JM. 2004. Plant body weight-induced secondary growth in Arabidopsis and its transcription phenotype revealed by whole-transcriptome profiling. *Plant Physiology* 135: 1069–1083.
- Krueck M, Trochta J, Cibulka M, Kral K. 2019. Beyond the cones: how crown shape plasticity alters aboveground competition for space and light—evidence from terrestrial laser scanning. *Agricultural and Forest Meteorology* 264: 188–199.
- Lehnbach R, Beyer R, Letort V, Heuret P. 2018. The pipe model theory half a century on: a review. *Annals of Botany* 121: 1427.
- Lenard E. 2008. Habits of trees and shrubs in landscape design. *Architecture. Civil Engineering Environment* (4): 13–20.
- Leonardi C, Stagi F. 2019. *L'architecture des arbres*. Paris, France: Fondation Cartier.
- Levernier N, Pouliquen O, Forterre Y. 2021. An integrative model of plant gravitropism linking statoliths position and auxin transport. *Frontiers in Plant Science* 12. doi: 10.3389/fpls.2021.651928.
- Li DHW. 2010. A review of daylight illuminance determinations and energy implications. *Applied Energy* 87: 2109–2118.
- Maddoni GA, Otegui ME, Andrieu B, Chelle M, Casal JJ. 2002. Maize leaves turn away from neighbors. *Plant Physiology* 130: 1181–1189.
- Mao TY, Zhu HH, Liu YY, Bao MZ, Zhang JW, Fu Q, Xiong CF, Zhang J. 2020. Weeping candidate genes screened using comparative transcriptomic analysis of weeping and upright progeny in an F1 population of *Prunus mume*. *Physiologia Plantarum* 170: 318–334.
- Marin-Buzon C, Perez-Romero A, Tucci-Alvarez F, Manzano-Agugliaro F. 2020. Assessing the orange tree crown volumes using google maps as a low-cost photogrammetric alternative. *Agronomy-Basel* 10: 893.
- McKim SM. 2020. Moving on up – controlling internode growth. *New Phytologist* 226: 672–678.
- McMahon T, Kronauer RE. 1976. Tree structures: deducing the principle of mechanical design. *Journal of Theoretical Biology* 59: 443–466.
- McSteen P, Leyser O. 2005. Shoot branching. *Annual Review of Plant Biology* 56: 353–374.
- Meneses BM, Lopes A. 2017. An integrated approach for wind fields assessment in coastal areas, based on bioindicators, CFD modeling, and observations. *Theoretical and Applied Climatology* 128: 301–310.
- Meroz Y, Silk WK. 2020. By hook or by crook: how and why do compound leaves stay curved during development? *Journal of Experimental Botany* 71: 6189–6192.
- Morita MT. 2010. Directional Gravity Sensing in Gravitropism. *Annual Review of Plant Biology* 61: 705–720.
- Moulia B, Bastien R, Chauvet-Thiry H, Leblanc-Fournier N. 2019. Posture control in land plants: growth, position sensing, proprioception, balance, and elasticity. *Journal of Experimental Botany* 70: 3467–3494.
- Moulia B, Combes D. 2004. Thigmomorphogenetic acclimation of plants to moderate winds greatly affects height structure in field-grown alfalfa (*Medicago sativa* L.), an indeterminate herb. *Comparative Biochemistry and Physiology Part A: Molecular & Integrative Physiology* 137: 77-A10-72.
- Moulia B, Coutand C, Julien JL. 2015. Mechanosensitive control of plant growth: bearing the load, sensing, transducing, and responding. *Frontiers in Plant Science* 6. doi: 10.3389/fpls.2015.00052.
- Moulia B, Douady S, Hamant O. 2021. Fluctuations shape plants through proprioception. *Science* 372: eabc6868.
- Moulia B, Fournier M, Guitard D. 1994. Mechanics and form of the maize leaf – *In vivo* qualification of flexural behaviour. *Journal of Materials Science* 29: 2359–2366.
- Moulia B, Fournier M. 1997. Optimal mechanical design of plant stems: the models behind the allometric power laws. In: Jeronimidis G, Vincent JFV, eds. *2<sup>nd</sup> international plant biomechanics conference*. Reading, UK: Centre for Biomechanics, University of Reading, 43–55.
- Moulia B, Fournier M. 2009. The power and control of gravitropic movements in plants: a biomechanical and systems biology view. *Journal of Experimental Botany* 60: 461–486.

- Moulton DE, Lessinnes T, Goriely A. 2020. Morphoelastic rods III: differential growth and curvature generation in elastic filaments. *Journal of the Mechanics and Physics of Solids* 142. doi: 10.1016/j.jmps.2020.104022.
- Muratov A, Baulin VA. 2015. Mechanism of dynamic reorientation of cortical microtubules due to mechanical stress. *Biophysical Chemistry* 207: 82–89.
- Murray JAH, Jones A, Godin C, Traas J. 2012. Systems analysis of shoot apical meristem growth and development: integrating hormonal and mechanical signaling. *The Plant Cell* 24: 3907–3919.
- Nagashima H, Hikosaka K. 2011. Plants in a crowded stand regulate their height growth so as to maintain similar heights to neighbours even when they have potential advantages in height growth. *Annals of Botany* 108: 207–214.
- Nagashima H, Hikosaka K. 2012. Not only light quality but also mechanical stimuli are involved in height convergence in crowded *Chenopodium album* stands. *New Phytologist* 195: 803–811.
- Nakamura M, Nishimura T, Morita MT. 2019. Gravity sensing and signal conversion in plant gravitropism. *Journal of Experimental Botany* 70: 3495–3506.
- Niklas KJ. 1994. *Plant allometry: the scaling of form and process*. Chicago, IL, USA: University of Chicago Press.
- Niklas KJ. 2013. Biophysical and size-dependent perspectives on plant evolution. *Journal of Experimental Botany* 64: 4817–4827.
- Niklas KJ, Cobb ED. 2017. Size-dependent variation in plant form. *Current Biology* 27: R900–R905.
- Niklas KJ, Spatz HC. 2004. Growth and hydraulic (not mechanical) constraints govern the scaling of tree height and mass. *Proceedings of the National Academy of Sciences, USA* 101: 15661–15663.
- Nikolov LA, Runions A, Das Gupta M, Tsiantis M. 2019. Leaf development and evolution. In: Grossniklaus U, ed. *Plant development and evolution*. San Diego, CA, USA: Elsevier Academic Press Inc, 109–139.
- Okamoto K, Ueda H, Shimada T, Tamura K, Kato T, Tasaka M, Morita MT, Hara-Nishimura I. 2015. Regulation of organ straightening and plant posture by an actin-myosin XI cytoskeleton. *Nature Plants* 1. doi: 10.1038/nplants.2015.31.
- Ortega JKE. 2018. Dimensionless numbers for plant biology. *Trends in Plant Science* 23: 6–9.
- Paul LK, Rinne PLH, van der Schoot C. 2014. Shoot meristems of deciduous woody perennials: self-organization and morphogenetic transitions. *Current Opinion in Plant Biology* 17: 86–95.
- Peyhardt J, Caraglio Y, Costes E, Lauri PE, Trotter C, Guedon Y. 2017. Integrative models for joint analysis of shoot growth and branching patterns. *New Phytologist* 216: 1291–1304.
- Poff KL. 1983. Perception of a unilateral light stimulus. *Philosophical Transactions of the Royal Society of London. Series B: Biological Sciences* 303: 479–487.
- Pouliquen O, Forterre Y, Berut A, Chauvet H, Bizet F, Legue V, Moullia B. 2017. A new scenario for gravity detection in plants: the position sensor hypothesis. *Physical Biology* 14. doi: 10.1088/1478-3975/aa6876.
- Prusinkiewicz P, Runions A. 2012. Computational models of plant development and form. *New Phytologist* 193: 549–569.
- Radoeva T, Weijers D. 2014. A roadmap to embryo identity in plants. *Trends in Plant Science* 19: 709–716.
- Ragni L, Greb T. 2018. Secondary growth as a determinant of plant shape and form. *Seminars in Cell & Developmental Biology* 79: 58–67.
- Roychoudhry S, Del Bianco M, Kieffer M, Kepinski S. 2013. Auxin controls gravitropic setpoint angle in higher plant lateral branches. *Current Biology* 23: 1497–1504.
- Roychoudhry S, Kepinski S. 2015. Shoot and root branch growth angle control – the wonderfulness of lateralness. *Current Opinion in Plant Biology* 23: 124–131.
- Roychoudhry S, Kieffer M, Del Bianco M, Liao CY, Weijers D, Kepinski S. 2017. The developmental and environmental regulation of gravitropic setpoint angle in Arabidopsis and bean. *Scientific Reports* 7. doi: 10.1038/srep42664.
- Runions A, Lane B, Prusinkiewicz P. 2007. Modeling trees with a space colonization algorithm. In: Ebert D, Mérillou S, eds. *Eurographics workshop on natural phenomena*. Aire-la-Ville, Switzerland: Eurographics Association, 63–70.
- Sato A, Sasaki S, Matsuzaki J, Yamamoto KT. 2014. Light-dependent gravitropism and negative phototropism of inflorescence stems in a dominant Aux/IAA mutant of *Arabidopsis thaliana*, axr2. *Journal of Plant Research* 127: 627–639.
- Schnablova R, Neustupa J, Woodard K, Klimesova J, Herben T. 2020. Disentangling phylogenetic and functional components of shape variation among shoot apical meristems of a wide range of herbaceous angiosperms. *American Journal of Botany* 107: 20–30.
- van der Schoot C, Paul LK, Rinne PLH. 2014. The embryonic shoot: a lifeline through winter. *Journal of Experimental Botany* 65: 1699–1712.
- Serrano-Mislata A, Sablowski R. 2018. The pillars of land plants: new insights into stem development. *Current Opinion in Plant Biology* 45: 11–17.
- Shibuya T, Takahashi S, Endo R, Kitaya Y. 2013. Height-convergence pattern in dense plant stands is affected by red-to-far red ratio of background illumination. *Scientia Horticulturae* 160: 65–69.
- Sierra-De-Grado R, Pando V, Martínez-Zurimendi P, Penalvo A, Bascones E, Moullia B. 2008. Biomechanical differences in the stem straightening process among *Pinus pinaster* provenances. A new approach for early selection of stem straightness. *Tree Physiology* 28: 835–846.
- Sievanen R, Raunonen P, Perttunen J, Nikinmaa E, Kaitaniemi P. 2018. A study of crown development mechanisms using a shoot-based tree model and segmented terrestrial laser scanning data. *Annals of Botany* 122: 423–434.
- Smith JM. 1978. Optimization theory in evolution. *Annual Review of Ecology and Systematics* 9: 31–56.
- Smith RS, Guyomarç'h S, Mandel T, Reinhardt D, Kuhlemeier C, Prusinkiewicz P. 2006. A plausible model of phyllotaxis. *Proceedings of the National Academy of Sciences, USA* 103: 1301–1306.
- Spicer R, Groover A. 2010. Evolution of development of vascular cambia and secondary growth. *New Phytologist* 186: 577–592.
- Tadrist L, Darbois-Texier B. 2016. Are leaves optimally designed for self-support? An investigation on giant monocots. *Journal of Theoretical Biology* 396: 125–131.
- Tardieu F. 2003. Virtual plants: modelling as a tool for the genomics of tolerance to water deficit. *Trends in Plant Science* 8: 9–14.
- Telewski FW. 2012. Is windswept tree growth negative thigmotropism? *Plant Science* 184: 20–28.
- Till-Bottraud I, de Villemeureuil P. 2016. Kin recognition or phenotype matching? *New Phytologist* 209: 13–14.
- Traas J. 2018. Molecular networks regulating meristem homeostasis. *Molecular Plant* 11: 883–885.
- Truskina J, Vernoux T. 2018. The growth of a stable stationary structure: coordinating cell behavior and patterning at the shoot apical meristem. *Current Opinion in Plant Biology* 41: 83–88.
- Ueda H, Tamura K, Hara-Nishimura I. 2015. Functions of plant-specific myosin XI: from intracellular motility to plant postures. *Current Opinion in Plant Biology* 28: 30–38.
- Vogelmann TC. 1993. Plant-tissue optics. *Annual Review of Plant Physiology and Plant Molecular Biology* 44: 231–251.
- Vos J, Evers JB, Buck-Sorlin GH, Andrieu B, Chelle M, de Visser PHB. 2010. Functional-structural plant modelling: a new versatile tool in crop science. *Journal of Experimental Botany* 61: 2101–2115.
- Waddington CH. 1957. *The strategy of the genes*. London, UK: George Allen & Unwin.
- Waite JM, Dardick C. 2018. *TILLER ANGLE CONTROL 1* modulates plant architecture in response to photosynthetic signals. *Journal of Experimental Botany* 69: 4935–4944.
- Wang B, Smith SM, Li JY. 2018. Genetic regulation of shoot architecture. *Annual Review of Plant Biology* 69: 437–468.
- Williams MW, Billingsley HD. 1970. Increasing number and crotch angles of primary branches of apple trees with cytokinins and gibberellic acid. *Journal of the American Society for Horticultural Science* 95: 649–+.
- Xu D, Qi X, Li JH, Han XJ, Wang JN, Jiang YZ, Tian YT, Wang YW. 2017. *PzTAC* and *PzLAZY* from a narrow-crown poplar contribute to regulation of branch angles. *Plant Physiology and Biochemistry* 118: 571–578.
- Yamamoto H, Yoshida M, Okuyama T. 2002. Growth stress controls negative gravitropism in woody plant stems. *Planta* 216: 280–292.
- Yoshihara T, Spalding EP. 2017. *LAZY* genes mediate the effects of gravity on auxin gradients and plant architecture. *Plant Physiology* 175: 959–969.
- Zheng TC, Li LL, Zhang QX. 2018. Advances in research on tortuous traits of plants. *Euphytica* 214. doi: 10.1007/s10681-018-2306-0.